Graphical Abstract

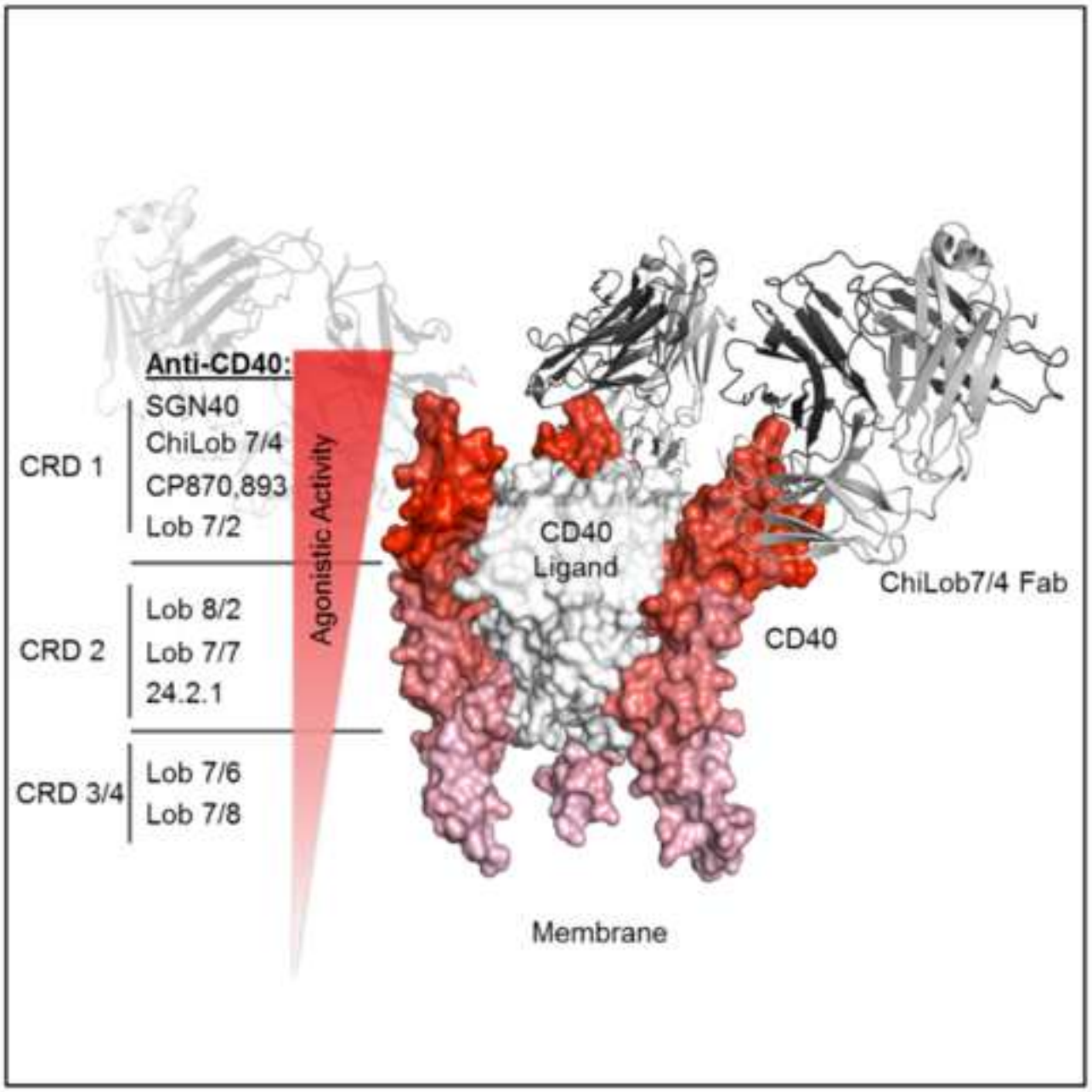

Complex interplay between epitope specificity and isotype dictates the biological activity of anti-human CD40 antibodies

Xiaojie Yu[1], H.T. Claude Chan[1], Christian M. Orr[1], Osman Dadas[1], Steven G.Booth[1], Lekh N Dahal[1], Christine A. Penfold[1], Lyn O'Brien[1,2], C. Ian Mockridge[1], Ruth R French[1], Patrick Duriez[3], Leon R. Douglas[3], Arwen R. Pearson[4], Mark S. Cragg[1,5], Ivo Tews[5,6], Martin J. Glennie[1*] and Ann L. White[1,7,8,9*].

[1]Antibody and Vaccine Group, Cancer Sciences Unit, University of Southampton Faculty of Medicine, SO16 6YD, UK; [2] Current address Dstl, Porton Down, Salisbury, SP4 0JQ, UK; Protein Core Facility, University of Southampton Faculty of Medicine, SO16 6YD, UK; [4]Hamburg Centre for Ultrafast Imaging & Institute for Nanostructure and Solid State Physics, University of Hamburg, 20146 Hamburg, Germany; [5]Institute for Life Sciences, University of Southampton, SO17 1BJ, UK; [6]Biological Sciences, University of Southampton, SO17 1BJ, UK; [7]Current address UCB-Celltech, 216 Bath Road, Slough, SL1 3WE, UK

[8] Lead contact; [9]To whom correspondence should be addressed: UCB-Celltech, 216 Bath Road, Slough, SL1 3WE, UK; ann.white@UCB.com

*Joint senior authors

Running title: Epitope, isotype and anti-CD40 mAb function

SUMMARY

Anti-CD40 monoclonal antibodies (mAb) that promote or inhibit receptor function hold promise as therapeutics for cancer and autoimmunity. Rules governing their diverse range of functions, however, are lacking. Here we determined characteristics of nine hCD40 mAb engaging epitopes throughout the CD40 extracellular region expressed as varying isotypes. All mAb formats were strong agonists when hyper-crosslinked, however only those binding the membrane-distal cysteine rich domain (CRD) 1 retained agonistic activity with physiological FcγR-crosslinking or as human IgG2 isotype; agonistic activity decreased as epitopes drew closer to the membrane. Additionally, all CRD2-4 binding mAb blocked CD40 ligand interaction and were potent antagonists. Thus the membrane distal CRD1 provides a region of choice for selecting CD40 agonists while CRD2-4 provides antagonistic epitopes.

Significance

Monoclonal antibodies (mAb) that regulate immune responses are providing potent therapeutics for treating cancer and autoimmune disease. One target in development is CD40, a Tumor Necrosis Factor Receptor (TNFR) superfamily member expressed on antigen presenting cells involved in regulating adaptive immunity. mAb targeting this receptor show diverse activities, from strong-agonism to powerful antagonism, however the rules determining activity are unclear. Here we demonstrate that a complex interplay between the location of the mAb epitope within CD40 and the isotype determine these differing levels of activity. Such detailed understanding of mAb mechanism of action will help guide the development of the next generation of immuno-therapeutics targeting CD40 and potentially other members of the TNFR superfamily.

INTRODUCTION

Monoclonal antibody (mAb) that target regulatory receptors to modulate immune responses are revolutionising the treatment of cancer and autoimmune disease (Chan and Carter, 2010; Schaer et al., 2014; Sharma and Allison, 2015). One promising target is CD40, a member of the Tumor Necrosis Factor Receptor Superfamily (TNFRSF) expressed on cells including B cells and specialised antigen presenting cells (Grewal and Flavell, 1998). Agonistic mAb that stimulate CD40 signalling are in development as cancer therapeutics designed to potentiate anti-tumor immunity (Remer et al., 2017; Vonderheide and Glennie, 2013), with the most encouraging results coming with CP870,893 in pancreatic cancer (Beatty et al., 2011). Conversely, antagonistic mAb that inhibit CD40 function are under investigation for the treatment of autoimmune and inflammatory conditions (Croft et al., 2013). The rules that govern whether a particular mAb will possess agonistic or antagonistic properties, however, are currently unclear.

The ligand for CD40 (CD40L/CD154) is trimeric and believed to initiate CD40 activation by clustering the receptor in the cell membrane allowing recruitment of TNFR associated factors (TRAFs) leading to immune activation (Werneburg et al., 2001). We have investigated the pathways by which agonistic anti-human (h) CD40 mAb can mimic this process and have demonstrated two distinct mechanisms, both influenced by the mAb constant region (White et al., 2015; White et al., 2011). The first is mediated by hyper-crosslinking of the mAb Fc through interaction with Fc gamma receptors (FcγR) (White et al., 2011). In *in vivo* mouse models cross-linking is mediated by the inhibitory FcγR, FcγRIIB. The anti-mouse (m) CD40 mAb 3/23 (White et al., 2011) and IC10 (Li and Ravetch, 2011) are agonistic when expressed as isotypes that engage mouse FcγRIIB with relatively high affinity (mouse IgG1 (m1) or rat IgG2a (r2a)) but not as isotypes with low FcγRIIB affinity (m2a or human IgG1 (h1)) or in

the absence of FcγRIIB expression (Li and Ravetch, 2011; White et al., 2011). FcγRIIB is thought to act as a hyper-crosslinking scaffold for the mAb to enhance clustering of CD40 in the membrane (Beers et al., 2016; White et al., 2013). Its predominant role *in vivo* likely reflects its bioavailability as other FcγR can mediate this function *in vitro*, at least when expressed at sufficient surface density (White et al., 2011; Wilson et al., 2011)

The second mechanism through which hCD40 mAb can elicit activity is independent of FcγR but dependent upon the hinge region of human IgG2 (h2) (White et al., 2015). h2 can adopt alternative disulphide bonding arrangements in its hinge that exhibit differences in flexibility and conformation (Dillon et al., 2008; Martinez et al., 2008; Wypych et al., 2008). We previously demonstrated that the hCD40 mAb ChiLob 7/4 becomes highly agonistic in the absence of FcγR-mediated hyper-crosslinking when 'locked' in an h2 'B' conformation where the two F(ab) arms are disulphide-linked to the hinge (Allen et al., 2009; White et al., 2015). h2B can agonise the receptor *in vivo* when administered as a $F(ab')_2$ fragment, potently stimulating antigen (Ag)-specific CD8 T cell proliferation in wild-type (WT) or *Fcgr2b*$^{-/-}$ (KO) mice, unequivocally demonstrating its FcγR-independent activity. Similarly, $F(ab')_2$ fragments of the clinical h2 hCD40 mAb CP870,893 also retain agonistic activity (Richman and Vonderheide, 2014) confirming that FcγR-mediated hyper-crosslinking is not obligatory for hCD40 mAb activity.-We hypothesise that the compact h2B conformation promotes close packaging of CD40 molecules in the membrane allowing efficient TRAF recruitment and receptor activation even when FcγR are absent (Beers et al., 2016; White et al., 2015).

These isotype-dependent rules of agonistic activity have been shown for multiple mAb targeting CD40 and other TNFR (Li and Ravetch, 2011; Li and Ravetch, 2012; White et al., 2015; Wilson et al., 2011; Xu et al., 2003), suggesting a common mechanism of action.

However, they were established by dissecting modes of activity of known agonists. It is not clear whether all mAb directed against CD40 or other TNFRSF members will be agonistic as m1 or h2 isotypes, or whether additional factors dictate activity. In particular, although epitope specificity clearly plays an important role in anti-hCD40 mAb function (Barr and Heath, 2001; Bjorck et al., 1994; Ellmark et al., 2002; Malmborg Hager et al., 2003; Yamniuk et al., 2016) the interaction between isotype and epitope in dictating anti-TNFR mAb activity has not been systematically investigated. Likewise, the rules governing antagonistic anti-hCD40 mAb behaviour are not clear. True antagonism likely necessitates the ability to prevent CD40L-mediated receptor activation suggesting that epitope specificity and the ability to prevent CD40L binding are inter-related.

The goal of this study was to define the relationship between epitope location and isotype in dictating the biological activity of hCD40 mAb.

RESULTS

Epitope and agonist activity

To examine the role of epitope specificity in the agonistic activity of hCD40 mAb we assembled a panel of nine mAb expressed with the m1 constant domain known to confer agonistic activity through FcγRIIB engagement (Li and Ravetch, 2011; White et al., 2011). We then compared their ability to stimulate B cell proliferation *in vitro* and CD8 T cell expansion *in vivo*. Three of these mAb, Lob 7/4-m1, SGN40-m1 and CP870,893-m1 were derived from ChiLob 7/4, SGN40 (dacetuzumab) and CP870,893, respectively, all of which have been used in clinical trials (Hussein et al., 2010; Johnson et al., 2015; Vonderheide et al., 2007). The remainder were produced in-house by standard hybridoma technology (Lob 7/8-m1, Lob 7/6-m1, Lob 8/2-m1, Lob 7/7-m1, Lob 7/2-m1) or generated from patent sequences (24.2.1-m1; US patent 2009/0130715).

Figure 1A shows the dose-dependent proliferation of purified human CD40 transgenic (hCD40Tg) mouse B cells expressing (WT) or lacking (KO) mFcγRII in response to the three clinical mAb. Lob 7/4-m1 and SGN40-m1 showed similar agonistic activity that was largely dependent upon crosslinking by the B cell FcγRII (Figure 1A). In contrast, CP870,893-m1 displayed much stronger agonistic activity, delivering 2-3 times more B cell proliferation with WT cells, and with much less dependence on crosslinking by mFcγRII.

Comparison of the remaining hCD40 mAb in the B cell proliferation assay revealed a spectrum of activity (Figure 1B) with WT B cells (left bars) ranging from strong agonists (CP870,893-m1) to those with little or no activity (Lob 7/8-m1). When mFcγRII KO B cells were used (middle bars), only CP870,893-m1 continued to show strong activity (Figure 1B). However, importantly, when a feeder layer of CHO-K1 cells over-expressing hFcγRIIB (XL) was included in these cultures (White et al., 2011) all of the mAb became highly agonistic,

demonstrating their capacity to bind CD40 and provide potent agonism in the presence of non-physiological levels of mFcγRII-mediated crosslinking.

To compare *in vivo* immunostimulatory activity, a vaccination model that measured SIINFEKL-specific CD8 (OT1) T cell responses against co-administered OVA in hCD40Tg mice was used (Figure 1C). The ability of the mAb to expand OT1 cells correlated with their relative activity in the B cell proliferation assay suggesting that similar rules dictate the agonistic activity of the mAb on distinct cell types (B cells and T cells) and also *in vitro* and *in vivo*.

ChiLob 7/4, SGN40 and CP870,893 engage similar epitopes in CRD1

The differences between mAb in both the level of agonistic activity and mFcγRII-dependency prompted us to examine more closely the role of epitope in agonism. To precisely define the epitope bound by ChiLob 7/4 we determined the crystal structure of its Fab' bound to soluble CD40 extracellular domain (Figure 2A, Table S1). Residues 1 to 211 of the ChiLob 7/4 light chain (LC) and 1 to 223 of the heavy chain (HC) were resolved (with the exception of residues 139-144 within CH1 of the HC). This leaves 3 terminal residues in the light chain and an estimated 15 terminal residues in the heavy chain unresolved in the electron density (see STAR Methods). CD40 was resolved in electron density for residues 21 to 120, corresponding to cysteine rich domain (CRD) 1, CRD2 and the majority of CRD3 (Figure 2A). The structure revealed that ChiLob 7/4 engaged an epitope at the N terminus of CD40 within CRD1 (Figure 2B). The complementarity determining region (CDR) 3 of the ChiLob 7/4 HC formed interactions with CD40 giving the highest ΔG, as analysed by PISA (Krissinel and Henrick, 2007), mostly within the A1 region of CRD1 (Figure 2B). The LC

CDR1 and CDR3 contacted the B2 region of CRD1, whilst the CDR2 region contacted both the CRD1 A1 and B2 regions (Figure 2B).

Western blotting and competition experiments by surface plasmon resonance (SPR) and flow cytometry were used to map the binding epitopes of other hCD40 mAb. ChiLob 7/4, SGN40 and CP870,893 all bound the full length CD40 extracellular domain (ECD), but not truncated forms where CRD1 was deleted (Figure 3A), and hence must recognise epitopes on CRD1 as reported previously for SGN40 and CP870,893 (Bjorck et al., 1994; Gladue et al., 2011). The mAb 24.2.1 bound to CD40 even when CRD1 was deleted, whereas Lob 7/6 bound when both CRD1 and CRD2 were deleted (Figure 3A). Flow cytometry data confirm domain-specific engagement as the CRD1 specific mAb Lob 7/4, SGN40 and CP870,893 all inhibited binding of Lob 7/4-FITC to hCD40Tg B cells, whereas Lob 7/6 and 24.2.1 that bind CRD domains closer to the membrane did not (Figure 3B top panels). In contrast, Lob 7/6 and 24.2.1 blocked labelling of hCD40Tg B cells with Lob 7/6-FITC whereas Lob 7/4, SGN40 and CP870,893 did not (Figure 3B, bottom panels). Furthermore, SPR showed that ChiLob 7/4, SGN40 and CP870,893 cross-competed with each other but not with Lob 7/6 for CD40 binding (Figure 3C). Thus, despite being associated with markedly different levels of agonistic activity (Figure 1), ChiLob 7/4, SGN40 and CP870,893 all bound to a similar region of CRD1 within CD40.

To differentiate the epitopes of ChiLob 7/4, SGN40 and CP870,893, we used a further deletion variant of CD40 in which the A1 domain of CRD1 was removed (residues 23-37, Figure 2A). The binding of the mAb to cells transfected with these variants was compared. ChiLob 7/4, SGN40 and CP870,893 that engage an epitope in CRD1 as well as 24.2.1 and Lob 7/6 that engage epitopes in CRD2-4 all bound approximately 80% of cells transfected with WT CD40 (Figure 3D). For the CD40-A1 deletion variant, 24.2.1 and Lob 7/6 still bound close to 80% of the cells, suggesting stable expression of this mutant. In contrast,

binding of SGN40 was reduced to 58%, binding of ChiLob 7/4 was reduced to 9%, and binding of CP870,893 was completely lost (Figure 3D). These data reflect an epitope variation for these mAb. In a simple modelling exercise based on the determined crystallographic structure of ChiLob 7/4, we demonstrate how these differences can be rationalised (Figure S1A). The modelling suggests that an interaction with CRD1 is lost while another interaction with CRD2 is gained, placing the binding epitope for SGN40 further down the CD40 scaffold compared to the one seen in the structure of ChiLob 7/4:CD40.

Western blotting and flow cytometry were used to produce epitope maps for a further six anti-hCD40 mAb (Lob 7/2, Lob 7/4, Lob 7/6 Lob 7/7, Lob 7/8, Lob 8/2 and 24.2.1: Figure S1B, S1C). The proposed distribution of these epitopes in relation to the CD40 domain structure is presented in Figure 3E.

Surface alanine scanning mutagenesis was used to confirm and refine these observations (Figure 4). CHO-K1 cells stably transfected with CD40 proteins in which consecutive pairs of surface amino acids were mutated to alanine were used to define residues critical for mAb binding. Consistent with the data in Figure 3, residues R27 and E28 close to the N-terminus of CD40 were found to be essential for CP870,893 binding, whereas ChiLob 7/4 was dependent upon residues F54 and T55 within the B2 domain of CRD1 (Figure 4). SGN40 and Lob 7/2 bound epitopes related to that of ChiLob 7/4, being additionally dependent upon residues E56 and T57 (Figure 4). This technique also identified residues in CRD2 important for the binding of Lob 8/2 (G63 E64 K94 G95) and Lob 7/7 (D84 P85) (Figure 4). Overall these data gave a detailed positional map of the binding sites on extracellular CD40 for each of the antibodies.

When the defined epitope locations are correlated with agonistic activity (Figure 1), it is clear that without extensive crosslinking only those mAb that bind to CRD1 are strong agonists.

The inability of mAb that bind epitopes in CRD2-4 to agonise CD40 may reflect reduced availability of their Fc regions to engage FcγR expressed at physiological levels. This notion was supported by experiments that demonstrated CRD2-4 binding mAb were also less able to direct macrophage mediated phagocytosis of opsonised B cells compared with CRD1 binders, a process that also requires FcγR interaction (Figure S2), as well as the strong agonism displayed by all antibodies when cross-linking was forced by super-physiological levels of mFcγRII (Figure 1B).

The influence of human isotype on epitope-dependent agonism

Having established the role of epitope in the context of the m1 isotype, we next explored the influence of epitope specificity in the context of human IgG isotypes, h1 and h2. As previously demonstrated (White et al., 2015) ChiLob 7/4-h2 and SGN40-h2 (mAb expressed with h2 constant domains) caused proliferation of isolated hCD40Tg mouse B cells, whereas their h1 counterparts were largely inactive (Figure 5A).

The activity of CP870,893 was largely independent of isotype with both h1 and h2 formats driving robust B cell expansion (Figure 5A). Moreover, the overall level of agonistic activity observed with CP870,893 was higher than either ChiLob 7/4-h2 or SGN40-h2, with >4-30 fold greater B cell proliferation at 1μg/ml depending upon the isotype and consistent with clinical studies demonstrating an approximately 10-fold lower maximum tolerated dose for CP870,893 versus SGN40 or ChiLob 7/4 (Hussein et al., 2010; Johnson et al., 2015; Vonderheide et al., 2007). The increased agonistic activity of CP870,893 was not due to enhanced CD40 binding as similar amounts of each mAb bound to B cells over the concentration range analysed (data not shown). This is further indication of the different mode of action of CP870,893.

Similar differences were observed in the ability of the different mAb to activate isolated human B cells, as assessed by CD23 upregulation (Figure 5B). Additionally, all h1 and h2 mAb activated human B cells equivalently when cells expressing super-physiological levels of hFcγRIIB were added (Figure 5B) suggesting similar mechanisms of CD40 activation in mouse and human B cells.

We next extended the panel of h1 and h2 hCD40 mAb to investigate how epitope specificity influenced agonism (Figure 5C). As with m1, we found that B cell agonistic activity was largely confined to those mAb binding to the CRD1 membrane distal domain. Lob 8/2 was the exception in that it bound to CRD2 but was agonistic, at least as h2. For all agonists, h2 was the most active of the human isotypes, particularly in the case of Lob 7/2, SGN40 and Lob 7/4, where h2 and m1 showed very similar agonism with h1 less active. However, the most striking difference between isotypes was seen when using mFcγRII KO B cells where in almost all cases h1 and m1 completely lost activity, while h2 retained agonistic function. An exception was the low level of agonism observed with Lob 7/2 h1 that was retained in the absence of mFcγRII. This is consistent with previous findings that h2 agonistic activity is independent of FcγR interaction (White et al., 2015). Finally, CP870,893 was again shown to be unique in evoking very high agonistic activity irrespective of isotype, and in retaining appreciable activity in the absence of mFcγRII. This distinct isotype insensitivity, compared with other mAb such as ChiLob 7/4, was recapitulated in an NF-κB activation assays (Figure S3).

To extend these studies *in vivo* we performed adoptive transfer of OT1 cells into hCD40 Tg mice (Figure 5D). As with the m1 of these reagents (Figure 1), the *in vitro* and *in vivo* data corresponded closely. ChiLob 7/4-h2 and SGN40-h2 stimulated strong expansion of OT1 T cells, whereas h1 was significantly less active (Figure 5D). This was particularly striking for

SGN40 where compared with h2, h1 showed very little activity. Importantly, and unlike m1 (Figure 1C), the activity of ChiLob 7/4-h2 and SGN40-h2 was independent of mFcγRII, showing comparable activity in mFcγRII KO mice, and confirming previous observations where $F(ab')_2$ fragments of ChiLob 7/4 h2 demonstrated wholly FcγR-independent activity in vivo (White et al 2015). In comparison, CP870,893 stimulated greater expansion of OT1 T cells as h1 or h2 compared with SGN40 and ChiLob 7/4 in the presence or absence of FcγRII. Thus, in contrast to ChiLob 7/4 and SGN40, CP870,893 displayed much greater agonistic activity both *in vitro* and *in vivo* that was largely independent of isotype and mFcγRII engagement. Overall these data support the notion that mAb binding to epitopes closer to the cell membrane make weaker agonists, irrespective of how agonism is achieved, either through the h2 isotype or FcγRII engagement.

The unusual nature of CP870,893 was underlined when we examined the effect of different h2 isoforms on its agonistic activity. Previously we showed that the FcγR-independent agonistic activity of ChiLob 7/4-h2 was dependent on the h2B isoform which exists in unmodified h2 preparations when hinge region disulfide bonds are 'shuffled'(White et al., 2015). The h2A and h2B forms can be enriched by chemical skewing in different redox buffers or by introducing cysteine to serine mutations, which 'lock' the molecule in different conformations. Figure 6 shows that, similar to Lob 7/4 (White et al., 2015), the agonistic activity of the SGN40 was stronger both *in vitro* and *in vivo* when enriched as h2B versus h2A (Figure 6A-C). In contrast, CP870,893 was equally active as h2A or h2B produced through either skewing or mutagenesis (Figure 6A), both *in vitro* (Figure 6B) and *in vivo* (Figure 6C). These results underline the unusual ability of CP870,893 to retain agonistic activity in all isotypes and isoforms and without FcγR crosslinking.

mAb that engage CRD2-4 block CD40L and are antagonists.

Having established the factors regulating potent agonism, we next examined the requirements for antagonism in our panel of mAb by assessing their ability to inhibit CD40L-mediated B cell activation. Flow cytometry demonstrated that none of the mAb that engage CRD1 (ChiLob 7/4, SGN40, CP870,893 or Lob 7/2) prevented binding of CD40L to hCD40Tg mouse B cells (Figure 7A) while mAb that bound epitopes in CRD2-4 either partially (Lob 7/7) or completely (Lob 7/7, Lob 7/8, 24.2.1, and Lob 8/2) blocked CD40L binding. The structural superposition of our ChiLob 7/4:CD40 complex with the CD40:CD40L complex (PDB:3QD6) demonstrates that ChiLob 7/4 and the CD40L bind to different CRDs on opposite faces of CD40 (Figure 7B). Since ChiLob 7/4, SGN40 and CP870,893 compete for related epitopes in CRD1 (Figures 3 and 4), none of these mAb would be predicted to block the CD40-CD40L interaction. mAb that engage epitopes in CRD2-4 may, however, interfere with CD40L binding.

The ability to block CD40-CD40L interaction correlated with differences in antagonistic function. When added to hCD40Tg B cells, hexameric mCD40L, a form with potent agonistic properties (Haswell et al., 2001), activated the cells as measured by homotypic adhesion (Figure 7C, top panels), upregulation of CD23, CD86 and MHCII (Figure 7C, lower 3 panels) and enhanced B cell proliferation (Figure 7D). When m1 mAb binding CRD1 (ChiLob 7/4, SGN40, CP870,893 and Lob 7/2) were added together with CD40L, B cell activation (Figure 7C) and proliferation (Figure 7D) were increased compared with CD40L alone. In contrast, Lob 7/7, which partially blocks CD40L binding had no significant additive effect on CD40L-mediated B cell activation or proliferation (Figure 7C and Figure 7D), whereas Lob 8/2, Lob 7/8 and 24.2.1 that all prevent CD40-CD40L interaction inhibited B cell activation and division compared to CD40L alone (Figure 7C and Figure 7D).

Similar results were observed when h2 mAb were used (Figure 7E). Lob 7/4 and Lob 7/2 (CRD1 binders) were both agonistic in the absence of exogenous ligand and maintained robust B cell proliferation in its presence (Figure 7E). In contrast, 24.2.1 and Lob 7/6, which engage epitopes in CRD2-4 and compete for CD40L binding, were not agonistic alone and prevented activation by CD40L (Figure 7E). An exception, as noted for Figure 5C, was Lob 8/2 that, despite blocking CD40L interaction, enhanced B cell proliferation in both the presence and absence of CD40L when used as h2.

Collectively, our data suggest that agonistic hCD40 mAb do not compete with CD40L binding, and retain agonistic activity in its presence. In contrast, antagonistic anti-hCD40 mAb bind to CRD2-4 that are closer to the cell membrane and tend to block CD40L binding, and thus antagonise CD40L activity.

Discussion

Here, we performed a comprehensive analysis of the roles that epitope specificity and isotype play in mediating hCD40 mAb function. Using a panel of 9 hCD40 mAb, including three in clinical development, engaging epitopes throughout the length of CD40 and with a number of different IgG isotype frameworks we reveal a complex interplay between epitope location and isotype that produces a range of activities from antagonism to strong agonism. These insights provide the opportunity to fine-tune hCD40 mAb function for defined levels of activity as may be required for specific tissue locations or therapeutic circumstances.

Both epitope specificity (Barr and Heath, 2001; Bjorck et al., 1994; Ellmark et al., 2002; Malmborg Hager et al., 2003; Yamniuk et al., 2016) and isotype (Dahan et al., 2016; Li and Ravetch, 2011; White et al., 2013; White et al., 2015; White et al., 2011; White et al., 2014) have separately been shown to regulate hCD40 mAb function. However, how these factors combine to mediate the wide-ranging levels of activity had not been systematically addressed. Mouse IgG1 constant regions can promote CD40 mAb agonism through interaction with FcγRIIB mediating mAb crosslinking *in vitro* and *in vivo* (White et al., 2011). However, when our nine hCD40 mAb were expressed with the same m1 backbone, a range of activities was observed, from non-agonistic to strongly-agonistic, clearly demonstrating that m1 constant regions cannot confer stimulatory activity to anti-hCD40 mAb *per se*. Indeed, only those mAb engaging epitopes in CRD1 (ChiLob 7/4, SGN40, CP870,893 and Lob 7/2) were agonistic as m1, whereas those that bound CRD2-4 were not, demonstrating an essential role for epitope location.

Protein crystallography elucidated the precise epitope for ChiLob 7/4; close to the N-terminus of CD40, most distal from the cell membrane and on the opposite face of CD40 to the CD40L binding site. We propose the dependence on membrane-distal CRD1 binding epitopes for

m1-mediated agonistic activity reflects the requirement for the mAb Fc to engage FcγRII on adjacent cells (White et al., 2013). Whereas the Fc domains of mAb that bind CRD1 may be accessible to FcγRII, steric constraints may prevent optimal FcγR engagement for mAb that bind epitopes closer to the membrane. This hypothesis is supported by the similar dependence on hCD40 mAb epitope location for macrophage phagocytosis of B cells that is dependent upon activatory FcγR engagement. Dahan et al (Dahan et al., 2016) recently reported that the hCD40 mAb clone 40.1, which engages an epitope towards the N-terminus of CD40, induced greater T cell responses in hCD40Tg mice than clone 40.2, which binds further down the molecule and competes with CD40L for CD40 association. Introduction of Fc mutations to selectively enhance hFcγRIIB affinity increased the stimulatory activity of both clones, however the activity of 40.1 remained substantially greater even in this context (Dahan et al., 2016). In the current study, all m1 mAb, regardless of epitope location, became highly agonistic *in vitro* when crosslinking was forced through introduction of FcγRIIB hyper-expressing accessory cells, reminiscent of earlier studies by Pound *et al* (Pound et al., 1999) and more recently Yamniuk *et al* (Yamniuk et al., 2016). These data suggest that for mAb whose agonism is dependent upon FcγRIIB binding, activity level is governed by a combination of three factors: i) accessibility of the mAb Fc (determined by epitope location); ii) affinity of the mAb Fc for FcγRIIB; iii) level of FcγRIIB expression in the local microenvironment.

A similar relationship with epitope location was observed when agonistic activity was examined in the context of h2 constant regions that can confer FcγR-independent agonistic activity due to a unique arrangement of hinge disulphides (White et al., 2015). Similar to results with m1, h2 mAb that engaged epitopes in CRD1 were agonistic whereas two of three h2 mAb that engaged epitopes in CRD2-4 did not display agonistic function. The exception

was Lob 8/2 that bound an epitope in CRD2 and agonised CD40 when expressed as h2 but not when expressed as m1. These results suggest the relationships between epitope and agonistic activity are distinct for m1 and h2. Exactly how h2 anti-hCD40 mAb mediate CD40 activation in the absence of FcγR binding is not known and the subject of our ongoing research. Under physiological conditions, CD40 is activated through engagement by trimeric CD40L. Although trimerisation is believed to be required for activation, CD40 is thought to exist as pre-formed dimers or trimers in membranes of unstimulated cells (Chan et al., 2000; Smulski et al., 2013). Elegant studies using recombinant CD40L molecules of different stoichiometries have also demonstrated that higher order clustering of CD40 can enhance signal intensity to levels above those observed with trimeric ligand (Graves et al., 2014; Haswell et al., 2001). We hypothesise that h2B hCD40 mAb are compact and when they engage epitopes in CRD1 they are able to cluster pre-formed CD40 dimers or trimers in the membrane to promote signalling in the absence of additional crosslinking. This is similar to a model proposed for the agonistic death receptor 5 (DR5) mAb AMG 655 where co-crystallisation of receptor-ligand-AMG 655 complexes suggest the formation of higher order signalling complexes in the cell membrane (Graves et al., 2014). It is possible that mAb engaging epitopes in CRD2-4 disrupt pre-formed complexes and prevent this mechanism of activation. Consistent with this hypothesis, we found that CRD1 binding mAb retained B cell activation in response to CD40L, whereas those that engage CRDs 2-4 inhibit CD40L-mediated activation, as has been previously reported (Challa et al., 1999; Pound et al., 1999). Further studies will be required to delineate the precise mechanism of CD40 activation by h2 mAb. Importantly, however, and similar to m1, the presence of mFcγRII over-expressing cells rendered all h2 anti-hCD40 mAb highly agonistic regardless of epitope, consistent with the ability of hyper-crosslinking to force activation through non-physiological receptor clustering.

Dahan et al (Dahan et al., 2016) recently demonstrated that the relative agonistic activity of h1 and h2 hCD40 mAb in hCD40Tg mice is influenced by the repertoire of FcγR available for Fc cross-linking; in mice expressing all human FcγR, h1 versions of CP870,893 and Lob 7/4 became more active than their h2 counterparts due to the superior ability of h1 to engage human FcγRIIB. Previous studies have similarly demonstrated that the isotype dependence of hCD40 mAb is influenced by the local FcγR availability (White et al., 2011; Wilson et al., 2011). However, Dahan et al also proposed that FcγR crosslinking was a requirement for the agonistic activity of h2 anti-hCD40 mAb as deglycosylated CP870,893, with its reduced ability to engage FcγR (Tao and Morrison, 1989), lost activity *in vivo* (Dahan et al., 2016*)*. This contrasts with our own work (White et al., 2015) as well as that of Vonderheide and co-workers (Richman and Vonderheide, 2014). Those authors demonstrated that $F(ab')_2$ fragments of CP870,893, which *de facto* cannot engage FcγR, could activate human B cells to a similar extent to the parental h2 IgG *in vitro*, similar to our own studies with ChiLob 7/4 that demonstrated strong *in vivo* agonistic activity of h2 (but not h1) $F(ab')_2$ fragments in stimulating T cell responses against co-administered OVA (White et al., 2015). The present study clearly shows FcγR-independent agonistic activity of multiple h2 anti-hCD40 mAb (SGN40, CP870,893, Lob 7/2 and Lob 8/2) *in vitro* using FcγR deficient B cells, as well as FcgRIIB-independent *in vivo* activity.

While some general rules regarding the roles of epitope and isotype in anti-hCD40 mAb function can be imputed from this study and used to aid design of future therapeutic mAb with defined characteristics, it is clear that this relationship is not simple and other factors can influence activity. Multiple hCD40 mAb are in early clinical development and it will be important to elucidate the characteristics of each of these agents to optimise activity. The different agonistic mechanisms exhibited (m1 versus h2 versus isotype independent activity

of CP870,893) will also need to be investigated for differences in therapeutic efficacy and toxicity. CD40 is just one member of the TNFR superfamily, many others of which are also targets for therapeutic mAb development. Whether the rules revealed for CD40 will apply to these other targets that exhibit similarities in their mechanisms of activation,also remains to be seen. Other studies have shown epitope location plays a crucial role in the activity of mAb against the Ig family member CD28, with epitopes in the lateral C''D loop imparting 'super-agonistic' properties enabling T cell activation in the absence of TCR stimulation (Luhder et al., 2003). The mechanisms responsible are distinct from those involved in CD40 activation, but further highlight the complexities involved in developing agonistic mAb therapeutics compared to those designed to block receptor-ligand interactions.

As well as helping to design effective immunotherapeutics, the different properties exhibited by the range of hCD40 mAb in this study also provides a valuable toolbox with which to probe the biology of TNFR activation.

Acknowledgements

We would like to thank colleagues from the Cancer Sciences Unit who provided advice and technical support and the Biomedical Research Facility for animal husbandry. We thank Chris Holes at the Macromolecular Crystallisation Facility, Biological Sciences, and staff at the European Synchrotron Radiation Facility for access and excellent user support, and acknowledge support through MX1732 & MX1848. Funding was provided by CRUK grants C1477/A10834, C1477/A20537, C34999/A18087 and C328/A25139 as well as EU FP7 grant 602262-2.

Author contributions

X.Y. designed and performed experiments, analyzed and interpreted data and helped write the manuscript; H.T.C, C.O., I.T., O.D., S.B., L.N.D., P.D., L.R.D., C.P. L.O.B., C.I.M, R.R.F. generated or provided key reagents or performed and analyzed research; A.R.P. supervised data collection, analyzed data and edited the manuscript; IT performed crystallographic structure analysis, discussed and interpreted data, and wrote the manuscript; M.S.C. supervised data collection, discussed and interpreted data and edited the manuscript; M.J.G and A.W designed the study, analyzed and interpreted data and wrote the manuscript.

Declaration of interests

Mark S Cragg acts as a consultant for BioInvent and has received research funding from BioInvent, GSK, iTeos and Roche. Martin J Glennie acts as a consultant to a number of biotech companies and receives institutional payments and royalties from antibody patents and licenses. This work is related to patent Family WO 2015/145360 protecting antibodies containing modified IgG2 domains which elicit agonist or antagonistic properties.

References

Ahonen, C., Manning, E., Erickson, L. D., O'Connor, B., Lind, E. F., Pullen, S. S., Kehry, M. R., and Noelle, R. J. (2002). The CD40-TRAF6 axis controls affinity maturation and the generation of long-lived plasma cells. Nat Immunol *3*, 451-456.

Allen, M. J., Guo, A., Martinez, T., Han, M., Flynn, G. C., Wypych, J., Liu, Y. D., Shen, W. D., Dillon, T. M., Vezina, C., and Balland, A. (2009). Interchain disulfide bonding in human IgG2 antibodies probed by site-directed mutagenesis. Biochemistry *48*, 3755-3766.

Barr, T. A., and Heath, A. W. (2001). Functional activity of CD40 antibodies correlates to the position of binding relative to CD154. Immunology *102*, 39-43.

Beatty, G. L., Chiorean, E. G., Fishman, M. P., Saboury, B., Teitelbaum, U. R., Sun, W., Huhn, R. D., Song, W., Li, D., Sharp, L. L., *et al.* (2011). CD40 agonists alter tumor stroma and show efficacy against pancreatic carcinoma in mice and humans. Science *331*, 1612-1616.

Beers, S. A., Glennie, M. J., and White, A. L. (2016). Influence of immunoglobulin isotype on therapeutic antibody function. Blood *127*, 1097-1101.

Bjorck, P., Braesch-Andersen, S., and Paulie, S. (1994). Antibodies to distinct epitopes on the CD40 molecule co-operate in stimulation and can be used for the detection of soluble CD40. Immunology *83*, 430-437.

Boross, P., Arandhara, V. L., Martin-Ramirez, J., Santiago-Raber, M. L., Carlucci, F., Flierman, R., van der Kaa, J., Breukel, C., Claassens, J. W., Camps, M., *et al.* (2011). The

inhibiting Fc receptor for IgG, FcgammaRIIB, is a modifier of autoimmune susceptibility. J Immunol *187*, 1304-1313.

Bulek, A. M., Madura, F., Fuller, A., Holland, C. J., Schauenburg, A. J., Sewell, A. K., Rizkallah, P. J., and Cole, D. K. (2012). TCR/pMHC Optimized Protein crystallization Screen. J Immunol Methods *382*, 203-210.

Challa, A., Pound, J. D., Armitage, R. J., and Gordon, J. (1999). Epitope-dependent synergism and antagonism between CD40 antibodies and soluble CD40 ligand for the regulation of CD23 expression and IgE synthesis in human B cells. Allergy *54*, 576-583.

Chan, A. C., and Carter, P. J. (2010). Therapeutic antibodies for autoimmunity and inflammation. Nat Rev Immunol *10*, 301-316.

Chan, F. K., Chun, H. J., Zheng, L., Siegel, R. M., Bui, K. L., and Lenardo, M. J. (2000). A domain in TNF receptors that mediates ligand-independent receptor assembly and signaling. Science *288*, 2351-2354.

Croft, M., Benedict, C. A., and Ware, C. F. (2013). Clinical targeting of the TNF and TNFR superfamilies. Nat Rev Drug Disc *12*, 147-168.

Dahan, R., Barnhart, B. C., Li, F., Yamniuk, A. P., Korman, A. J., and Ravetch, J. V. (2016). Therapeutic Activity of Agonistic, Human Anti-CD40 Monoclonal Antibodies Requires Selective FcgammaR Engagement. Cancer Cell *29*, 820-831.

Dillon, T. M., Ricci, M. S., Vezina, C., Flynn, G. C., Liu, Y. D., Rehder, D. S., Plant, M., Henkle, B., Li, Y., Deechongkit, S., *et al.* (2008). Structural and functional characterization of disulfide isoforms of the human IgG2 subclass. J Biol Chem *283*, 16206-16215.

Ellmark, P., Ottosson, C., Borrebaeck, C. A., Malmborg Hager, A. C., and Furebring, C. (2002). Modulation of the CD40-CD40 ligand interaction using human anti-CD40 single-chain antibody fragments obtained from the n-CoDeR phage display library. Immunology *106*, 456-463.

Emsley, P., Lohkamp, B., Scott, W. G., and Cowtan, K. (2010). Features and development of Coot. Acta crystallographica Section D, Biological crystallography *66*, 486-501.

Evans, P. R., and Murshudov, G. N. (2013). How good are my data and what is the resolution? Acta crystallographica Section D, Biological crystallography *69*, 1204-1214.

Gladue, R. P., Paradis, T., Cole, S. H., Donovan, C., Nelson, R., Alpert, R., Gardner, J., Natoli, E., Elliott, E., Shepard, R., and Bedian, V. (2011). The CD40 agonist antibody CP-870,893 enhances dendritic cell and B-cell activity and promotes anti-tumor efficacy in SCID-hu mice. Cancer Immunol Immunother *60*, 1009-1017.

Graves, J. D., Kordich, J. J., Huang, T. H., Piasecki, J., Bush, T. L., Sullivan, T., Foltz, I. N., Chang, W., Douangpanya, H., Dang, T., *et al.* (2014). Apo2L/TRAIL and the death receptor 5 agonist antibody AMG 655 cooperate to promote receptor clustering and antitumor activity. Cancer Cell *26*, 177-189.

Grewal, I. S., and Flavell, R. A. (1998). CD40 and CD154 in cell-mediated immunity. Annu Rev Immunol *16*, 111-135.

Haswell, L. E., Glennie, M. J., and Al-Shamkhani, A. (2001). Analysis of the oligomeric requirement for signaling by CD40 using soluble multimeric forms of its ligand, CD154. Eur J Immunol *31*, 3094-3100.

Hussein, M., Berenson, J. R., Niesvizky, R., Munshi, N., Matous, J., Sobecks, R., Harrop, K., Drachman, J. G., and Whiting, N. (2010). A phase I multidose study of dacetuzumab (SGN-40; humanized anti-CD40 monoclonal antibody) in patients with multiple myeloma. Haematologica *95*, 845-848.

Johnson, P., Challis, R., Chowdhury, F., Gao, Y., Harvey, M., Geldart, T., Kerr, P., Chan, C., Smith, A., Steven, N., *et al.* (2015). Clinical and biological effects of an agonist anti-CD40 antibody: a Cancer Research UK phase I study. Clin Cancer Res *21*, 1321-1328.

Kabsch, W. (2010). Xds. Acta crystallographica Section D, Biological crystallography *66*, 125-132.

Krissinel, E., and Henrick, K. (2007). Inference of macromolecular assemblies from crystalline state. J Mol Biol *372*, 774-797.

Li, F., and Ravetch, J. V. (2011). Inhibitory Fcgamma receptor engagement drives adjuvant and anti-tumor activities of agonistic CD40 antibodies. Science *333*, 1030-1034.

Li, F., and Ravetch, J. V. (2012). Apoptotic and antitumor activity of death receptor antibodies require inhibitory Fcgamma receptor engagement. Proc Natl Acad Sci *109*, 10966-10971.

Luhder, F., Huang, Y., Dennehy, K. M., Guntermann, C., Muller, I., Winkler, E., Kerkau, T., Ikemizu, S., Davis, S. J., Hanke, T., and Hunig, T. (2003). Topological requirements and signaling properties of T cell-activating, anti-CD28 antibody superagonists. J Exp Med *197*, 955-966.

Malmborg Hager, A. C., Ellmark, P., Borrebaeck, C. A., and Furebring, C. (2003). Affinity and epitope profiling of mouse anti-CD40 monoclonal antibodies. Scand J Immunol *57*, 517-524.

Martinez, T., Guo, A., Allen, M. J., Han, M., Pace, D., Jones, J., Gillespie, R., Ketchem, R. R., Zhang, Y., and Balland, A. (2008). Disulfide connectivity of human immunoglobulin G2 structural isoforms. Biochemistry *47*, 7496-7508.

McCoy, A. J., Grosse-Kunstleve, R. W., Adams, P. D., Winn, M. D., Storoni, L. C., and Read, R. J. (2007). Phaser crystallographic software. Journal of applied crystallography *40*, 658-674.
Murshudov, G. N., Vagin, A. A., and Dodson, E. J. (1997). Refinement of macromolecular structures by the maximum-likelihood method. Acta crystallographica Section D, Biological crystallography *53*, 240-255.

Pound, J. D., Challa, A., Holder, M. J., Armitage, R. J., Dower, S. K., Fanslow, W. C., Kikutani, H., Paulie, S., Gregory, C. D., and Gordon, J. (1999). Minimal cross-linking and

epitope requirements for CD40-dependent suppression of apoptosis contrast with those for promotion of the cell cycle and homotypic adhesions in human B cells. Int Immunol *11*, 11-20.

Remer, M., White, A., Glennie, M., Al-Shamkhani, A., and Johnson, P. (2017). The Use of Anti-CD40 mAb in Cancer. Curr Top Microbiol Immunol *405*, 165-207.

Richman, L. P., and Vonderheide, R. H. (2014). Role of crosslinking for agonistic CD40 monoclonal antibodies as immune therapy of cancer. Cancer Immunol Res *2*, 19-26.

Schaer, D. A., Hirschhorn-Cymerman, D., and Wolchok, J. D. (2014). Targeting tumor-necrosis factor receptor pathways for tumor immunotherapy. J Immunother Cancer *2*, 7.

Sharma, P., and Allison, J. P. (2015). Immune checkpoint targeting in cancer therapy: toward combination strategies with curative potential. Cell *161*, 205-214.

Smulski, C. R., Beyrath, J., Decossas, M., Chekkat, N., Wolff, P., Estieu-Gionnet, K., Guichard, G., Speiser, D., Schneider, P., and Fournel, S. (2013). Cysteine-rich domain 1 of CD40 mediates receptor self-assembly. J Biol Chem *288*, 10914-10922.

Tao, M. H., and Morrison, S. L. (1989). Studies of aglycosylated chimeric mouse-human IgG. Role of carbohydrate in the structure and effector functions mediated by the human IgG constant region. J Immunol *143*, 2595-2601.

Vonderheide, R. H., Flaherty, K. T., Khalil, M., Stumacher, M. S., Bajor, D. L., Hutnick, N. A., Sullivan, P., Mahany, J. J., Gallagher, M., Kramer, A., *et al.* (2007). Clinical activity and immune modulation in cancer patients treated with CP-870,893, a novel CD40 agonist monoclonal antibody. J Clin Oncol *25*, 876-883.

Vonderheide, R. H., and Glennie, M. J. (2013). Agonistic CD40 antibodies and cancer therapy. Clin Cancer Res *19*, 1035-1043.

Werneburg, B. G., Zoog, S. J., Dang, T. T., Kehry, M. R., and Crute, J. J. (2001). Molecular characterization of CD40 signaling intermediates. J Biol Chem *276*, 43334-43342.

White, A. L., Chan, H. T., French, R. R., Beers, S. A., Cragg, M. S., Johnson, P. W., and Glennie, M. J. (2013). FcgammaRIotaIotaB controls the potency of agonistic anti-TNFR mAbs. Cancer Immunol Immunother *62*, 941-948.

White, A. L., Chan, H. T., French, R. R., Willoughby, J., Mockridge, C. I., Roghanian, A., Penfold, C. A., Booth, S. G., Dodhy, A., Polak, M. E., *et al.* (2015). Conformation of the human immunoglobulin G2 hinge imparts superagonistic properties to immunostimulatory anticancer antibodies. Cancer Cell *27*, 138-148.

White, A. L., Chan, H. T., Roghanian, A., French, R. R., Mockridge, C. I., Tutt, A. L., Dixon, S. V., Ajona, D., Verbeek, J. S., Al-Shamkhani, A., *et al.* (2011). Interaction with FcgammaRIIB is critical for the agonistic activity of anti-CD40 monoclonal antibody. J Immunol *187*, 1754-1763.

White, A. L., Dou, L., Chan, H. T., Field, V. L., Mockridge, C. I., Moss, K., Williams, E. L., Booth, S. G., French, R. R., Potter, E. A., *et al.* (2014). Fcgamma receptor dependency of agonistic CD40 antibody in lymphoma therapy can be overcome through antibody multimerization. J Immunol *193*, 1828-1835.

Wilson, N. S., Yang, B., Yang, A., Loeser, S., Marsters, S., Lawrence, D., Li, Y., Pitti, R., Totpal, K., Yee, S., *et al.* (2011). An Fcgamma receptor-dependent mechanism drives antibody-mediated target-receptor signaling in cancer cells. Cancer Cell *19*, 101-113.

Winn, M. D., Ballard, C. C., Cowtan, K. D., Dodson, E. J., Emsley, P., Evans, P. R., Keegan, R. M., Krissinel, E. B., Leslie, A. G., McCoy, A., *et al.* (2011). Overview of the CCP4 suite and current developments. Acta crystallographica Section D, Biological crystallography *67*, 235-242.

Wypych, J., Li, M., Guo, A., Zhang, Z., Martinez, T., Allen, M. J., Fodor, S., Kelner, D. N., Flynn, G. C., Liu, Y. D., *et al.* (2008). Human IgG2 antibodies display disulfide-mediated structural isoforms. J Biol Chem *283*, 16194-16205.

Xu, Y., Szalai, A. J., Zhou, T., Zinn, K. R., Chaudhuri, T. R., Li, X., Koopman, W. J., and Kimberly, R. P. (2003). Fc gamma Rs modulate cytotoxicity of anti-Fas antibodies: implications for agonistic antibody-based therapeutics. J Immunol *171*, 562-568.

Yamniuk, A. P., Suri, A., Krystek, S. R., Tamura, J., Ramamurthy, V., Kuhn, R., Carroll, K., Fleener, C., Ryseck, R., Cheng, L., *et al.* (2016). Functional Antagonism of Human CD40 Achieved by Targeting a Unique Species-Specific Epitope. J Mol Biol *428*, 2860-2879.

Figure legends

Figure 1. Mouse IgG1 constant regions cannot confer agonistic activity to all anti-h CD40 mAb. (A) Purified hCD40Tg (WT) or hCD40Tg/*Fcgr2b*$^{-/-}$ (KO) splenic mouse B cells were incubated with increasing concentrations of Lob 7/4-m1, SGN40-m1 or CP870,893-m1 for 4 days, and proliferation measured by ^{3}H-thymidine incorporation. Mean ± SEM, n=3, data representative for at least 3 experiments. (B) Purified splenic WT or KO B cells in the absence or presence of irradiated hFcγRIIB-overexpressing CHO-K1 cells (XL) were treated as in A with 1 μg/ml each mAb (m1). Mean ± SEM, n=3, data representative of at least 3 experiments. (C) 1 x 10^5 OTI cells were adoptively transferred to hCD40Tg mice one day before treatment with 30 μg of the indicated mAb (m1). PE-labelled SIINFEKL +ve cells, expressed as percentage of total $CD8^+$ cells. Values for individual mice are shown; error bars represent mean ± SEM. Data representative of at least 2 experiments. Comparison of all CRD1-targeting mAb individually with Lob 7/6-m1, $^{**}p < 0.01$ using one way ANOVA followed by Tukey's multiple comparisons test.

Figure 2. Crystal structure of ChiLob 7/4 F(ab) in complex with CD40 extracellular domain. (A) The crystal structure of CD40:ChiLob 7/4 F(ab) complex shows the F(ab) in grey (dark grey – heavy chain, light grey – light chain) and CD40 coloured by CRD (blue - CRD1-A1, red - CRD1-B2 , green – CRD2-A1 , magenta – CRD2-B2 , orange - CRD3-A1 , cyan – CRD3-B2 (partial)). (B) Interface, with structural elements removed for clarity. Shown are the CDR loops of ChiLob 7/4 in red for CDR1, green for CDR2, and blue for CDR3. Light colour shades represent the light chain, dark shades the heavy chain. CD40 coloured as in A (translucent). See also Table S1.

Figure 3. Epitope mapping of anti-hCD40 mAb. (A) C-terminally His-tagged CD40 proteins consisting of 4, 3, or 2 CRD domains (4 = full length; 3 = CRD1 deleted; 2 = CRD1 and 2 deleted) were analysed by Western blotting with the mAb indicated above each panel used for detection. A composite image from multiple blots with different antibodies is shown. (B) hCD0Tg mouse B cells were incubated with FITC-labelled Lob 7/4 or Lob 7/6 as indicated in the absence or presence of a 10-fold excess of competitor (comp) mAb indicated above each plot. Cell labelling was assessed by flow cytometry; filled histogram, unlabelled cells; light grey, FITC-labelled mAb alone; black line, FITC-labelled mAb + competitor. (C) Surface plasmon resonance analysis of mAb competition for CD40 binding. The mAb indicated above each plot was flowed over immobilised hCD40 ECD for 800 seconds to allow saturation of hCD40 binding sites, followed by the addition of individual competitor mAb for 350 seconds. Non-competitive mAb (i.e. mAb without overlapping epitope) give a response greater than 500 RU. (D) Untransfected 293 cells (None), or cells transfected with full length (WT) human CD40 or CD40 in which N-terminal amino acids 23-37 had been deleted, were incubated with the indicated anti-hCD40 mAb, (h2 isotype). Bound mAb were detected with anti-human Fc-FITC. The percentage of cells in the boxed region, denoting positive staining, is shown for each plot. Results from 1 of 2 experiments shown. E. Schematic of the approximate locations of epitopes for nine human CD40 mAb analysed. See also Figure S1.

Figure 4. Alanine scanning epitope mapping of anti-hCD40 mAb. CHO-k1 cells stably expressing mutant hCD40 proteins were incubated with the indicated m1 mAb and binding detected by flow cytometry with anti-mouse Fc-FITC. (A) Example plots for the F54-T55 mutant to illustrate positive (tick) and negative (cross) binding results. (B) Summary of data for additional hCD40 mutants (at least two experiments per combination). (C) Deduced mAb

epitopes are illustrated on the hCD40 crystal structure resolved in Figure 2, and are colour-coded with those for ChiLob 7/4, SGN40 and Lob 7/2 overlapping. See also Figure S2.

Figure 5. Influence of human IgG isotype on epitope-dependent agonism. (A) Purified hCD40Tg mouse splenic B cells were incubated with the indicated mAb isotypes at various concentrations for 4 days, and proliferation was measured as in Figure 1A. Mean ± SEM, n= 3, data representative of at least 3 experiments. (B) Purified human B cells were incubated with the indicated mAb at 1 μg/ml in the absence (-) or presence (+) of cross linking cells over-expressing hFγRIIB, as in Figure 1B. Histograms show expression of CD23 (black lines) compared to untreated cells (grey histograms) as determined by flow cytometry. (C) Purified hCD40Tg WT or KO mouse splenic B cells were treated as in A with 1 μg/ml each mAb of m1, h1 or h2 isotype, and proliferation determined by ^{3}H-thymidine incorporation. Mean ± SEM, n= 5, data representative of at least 3 experiments. (D) 1 x 10^5 OT1 cells were adoptively transferred to hCD40Tg mice one day before treatment with 100 μg h1 or h2 of the indicated mAb and 100 μg OVA. OT1 cells in peripheral blood were quantified on day 5 using PE-labelled SIINFEKL tetramer, expressed as percentage of total $CD8^+$ cells. Data points represent individual animals from at least 2 independent experiments per mAb. Horizontal bars indicate mean values. **p<0.001, ****p<0.0001, h1 versus h2 of same mAb using the Student's unpaired t test**.** See also Figure S3.

Figure 6. Influence of hinge conformation on SGN40 and CP870,893 agonistic activity. (A) CE-SDS profiles of the mAb chemically skewed towards their h2A and h2B conformations (h2'A' and h2'B', respectively) or 'locked' in h2A (through point mutation C233S) and h2B (through point mutation C127S). (B) Ability of the different h2 mAb to stimulate proliferation of hCD40Tg mouse B cells was analysed as described in Figure 1A.

Data is presented as mean ± range of duplicate samples. (C) The ability of the mAb to stimulate OT1 cell expansion *in vivo* was analysed as described for Figure 1C. Results for individual animals are plotted. Horizontal bars indicate mean values. *$p<0.05$ for h2'A' versus h2'B' using the Student's unpaired t test.

Figure 7. Antagonist anti-hCD40 mAb engage CRD2-4 domains. (A) Purified hCD40Tg mouse splenic B cells were incubated with or without the indicated mAb, all of m1 isotype followed by hexameric mCD40L-h1Fc. Bound CD40L was then detected with anti-human-FITC and flow cytometry. (B) Structure superposition of CD40:Lob 7/4 F(ab) complex (coloured as in Figure 2A) with the CD40:CD40L complex (PDB:3QD6). CD40L is shown as a trimer binding to the opposite side of CD40 than Lob 7/4 and to a different CRD (CD40L shown as white surface representation). (C) Purified hCD40Tg mouse splenic B cells were incubated with CD40L alone (10 µg/ml) or together with the indicated mAb (m1 at 1 µg/ml) for 20 hours. Activation was assessed by homotypic adhesion (top) or flow cytometry to assess upregulation of activation markers. Results from one of at least 3 experiments for each mAb are shown. (D) Purified hCD40Tg mouse splenic B cells were incubated with the indicated mAb (m1 at 1 µg/ml) under control conditions (left panel) or in the presence of CD40L (10 µg/ml, right panel). Proliferation was assessed by ^{3}H-thymidine incorporation as in Figure 1A and plotted as mean ± SEM. (E) As in D, except that h2 mAb were used. Mean ± SEM of triplicate samples representing results from 2 or 3 experiments per mAb. **$p<0.01$, ***$p<0.001$ using the unpaired Student's t test, left hand plots for indicated groups, right hand plots versus CD40L alone.

STAR METHODS

CONTACT FOR REAGENT AND RESOURCE SHARING

Further information and requests for resources and reagents should be directed to and will be fulfilled by the Lead Contact, Ann L White (ann.white@UCB.com).

EXPERIMENTAL MODEL AND SUBJECT DETAILS

Mice

C57BL/6 mice were from Charles River Laboratories (Kent, UK). FcγRIIB$^{-/-}$ and FcRγ$^{-/-}$ C57BL/6 mice (Boross et al., 2011) were kindly provided by Dr Sjef Verbeek (Leiden University Medical School). OTI TCR transgenic mice were kindly provided by Dr Matthias Merkenschlager, (Imperial College, London) and human CD40 transgenic (hCD40 Tg) were kindly provided by Randolph Noelle (Kings College, London) (Ahonen et al., 2002). Human CD40 Tg/*Fcgr2b*$^{-/-}$ and hCD40Tg/*Fcer1g*$^{-/-}$ mice were generated by crossbreeding with genotypes confirmed by flow cytometry. Animals were bred and housed in local animal facilities, were fed regular chow and had freely accessible water. For all experiments, age- (predominantly 8-12 weeks) and sex-matched mice were used that were randomly assigned to experimental groups and housed together under the same conditions. All experiments were carried out according to local ethical committee guidelines under UK Home Office licence numbers PPL30/2451 and PPL30/2964.

Human Samples

PBMCs were obtained from healthy adult volunteers through Southampton National Blood Service after informed consent. As anonymized samples were used, the sex and age of the volunteers are not known. Density gradient centrifugation (Lymphoprep, Axis-Shield) was performed within 4 hours. Use of human samples was approved by the East of Scotland Research Ethics Service, in accordance with the declaration of Helsinki.

METHOD DETAILS

Antibodies and reagents.

Anti-mouse CD23-PE was from BD Biosciences. For OTI cell staining, anti-mouse CD8α–APC (clone 53-6.7; BD Biosciences), and PE- SIINFEKL tetramers were produced in-house as described previously (White et al., 2011). Chicken ovalbumin (OVA) was from Sigma-Aldridge (Poole, UK). Anti-mouse CD86-FITC (clone GL1) and anti-mouse MHCII-FITC (clone M5/114) were both produced in-house.

DNA constructs encoding heavy and light (kappa) chain variable regions of various mAb were either amplified from hybridomas by PCR or synthesized by Genewiz, Inc. The anti-hCD40 mAb SGN40, CP870,893 and 24.2.1 were produced using patent published sequences. Lob 7/2, Lob 7/4, Lob 7/6, Lob 7/7, Lob 7/8 and Lob 8/2 were produced in-house using standard hybridoma technology. Variable regions were subcloned into expression vectors (pEE6.4 for heavy chain and pEE12.4 vector for light chain, Lonza) containing constant regions of different antibody isotypes. Heavy and light chain vectors were subcloned together before transfection into 293F cells (for transient) or CHO-K1 cells (for stable) production of mAb. Secreted mAb were purified by Protein A-Sepharose (Sigma-Aldrich) chromatography and aggregates (as revealed by SEC-HPLC) removed by gel filtration through Sephadex 200 (Sigma-Aldrich). All preparations were endotoxin low (<1 ng/mg protein) as determined by an Endosafe-PTS portable test system (Charles River Laboratories). Non-reducing denaturing capillary electrophoresis (nrCE-SDS) of mAb preparations was performed using a Beckman PA800 Plus analyser according to the manufacturer's instructions. To produce skewed forms of h2, mAb were dialysed into 0.2 M Tris pH8.0 containing 6 mM cysteine plus 1 mM

cystamine with (for h2A) or without (for h2B) 2 M guanidine hydrochloride, for 4 days at 4^0C, then dialysed into PBS before use.

B cell activation and proliferation.

B cells were purified from mouse spleen or human PBMC using magnetic negative selection kits (StemCell Technologies). Cells were plated into 96-well round-bottom dishes at 1 x 10^5 cells/well with concentrations of mAb as described for individual experiments. In some cases, 1 x 10^5 irradiated CHO-K1 or 293F cells transfected with human FcγRIIB (White et al., 2011) were also added. To assess activation, cells were photographed (Olympus CKX41 microscope with CC12 soft imaging system) after 48 hour incubation and activation marker expression analysed by flow cytometry (FACSCalibur, BD Biosciences). Proliferation was assessed by [methyl-^{3}H] thymidine (PerkinElmer, Cambridge, UK) incorporation after 5 days of culture, as described (White et al., 2011).

Immunisation and assessment of immune responses.

To assess *in vivo* agonistic activity of anti-hCD40 mAb, 1 x 10^5 splenic OVA-specific CD8 (OT1) T cells were adoptively transferred via tail vein injection in 200 μl PBS; one day later, anti-hCD40 mAb (30 μg or 100 μg, see figure legends) and OVA (100 μg) were injected vial tail vein. Expansion of OT1 cells was monitored by serial blood sampling and of the number circulating enumerated by flow cytometry on a BD FacsCalibur using anti-CD8-APC and SIINFEKL-PE tetramer.

Generation and expression of CD40 constructs

A full-length CD40 extracellular domain (ECD) construct (residues 21-193) was generated by PCR using wild-type CD40 DNA as template. The genes for the coding regions of

truncated forms of CD40 and CD40-hisTag fusion proteins were synthesized from GeneArt and subcloned into pcDNA3.1 vector. FreeStyle 293F cells (Thermo Fisher) were transfected with constructs using a DNA:PEI (polyethylenimine, Polysciences) ratio of 1:3 and supernatant harvested for purification on day 7 using a Ni-NTA column (GE-Healthcare). To assess binding of mAb to recombinant proteins by western blot, protein samples were prepared in SDS loading buffer without DTT and ran on an 18% polyacrylamide gel. The proteins were transferred on nitrocellulose, the membrane blocked before probing with anti-hCD40 or anti-His mAb (Qiagen) at 4ºC overnight. The membrane was washed, then incubated with either goat anti-human Fc-HRP (Jackson Immuno Research) or polyclonal goat anti-mouse IgG-HRP (Dako), and washed before adding SuperSignal West Pico chemiluminescence substrate (Thermo Fisher). Signals were analysed using a Fluor-S Multi-imager Bio-Rad system.

Alanine scanning mutagenesis was carried out on the CRD1 and CRD2 domains of hCD40 to map CD40 mAb epitopes. The wild type extracellular and transmembrane domains of hCD40 were cloned into the pCIpuro vector (Promega) for cell surface expression. For scanning mutagenesis, sets of two consecutive residues were mutated to alanines. Nucleotide sequences were designed in house and synthesized by Genewiz (Hertfordshire, UK). CHO-K1 clones stably expressing each mutant were generated using GenePORTER Transfection reagent (Amsbio, UK) and 10 µg/ml puromycin (Invivogen, UK) for selection. Two different stable clones varying in the level of CD40 expression were generated for each mutant. For epitope mapping, 10 µg/ml of hCD40 m1 mAb was incubated with the cells on ice for 30 minutes before secondary detection using goat F(ab')2 anti-mouse Fc-FITC. The level of mAb binding was then assessed by flow cytometry (FACSCalibur) and data analysed by FCS Express V3 (De Novo Software).

Protein Crystallography

ChiLob 7/4-h1 was digested with pepsin (10 mg/ml at room temperature). Cleavage of the heavy chain occurs below the cysteine rich sequence of the hinge region. The cleaved product was subjected to size exclusion chromatography (SEC) using two coupled S200 columns (GE Healthcare; 70ml volume in total) to remove the Fc fragment. The resulting $F(ab')_2$ fragments were reduced with DTT to produce Fab' and quenched by Iodoacetamide. The final Fab' product was verified by HPLC and CE-SDS.

The Fab' fragment was incubated with CD40 ECD (CRD 1-4) in PBS at room temperature for 30 minutes at a molar ratio of 1:4 (CD40:Fab'), followed by SEC using an S200 10/300 column (GE Healthcare) using HEPES buffer (150 mM HEPES, 50 mM KCl pH 7.0). Complex formation was confirmed by HPLC. The complex was concentrated to 13.6 mg/ml for crystallisation in sitting drop plates, set up using a TOPS (Bulek et al., 2012) screen at 20°C using a Gryphon (Art Robbins Instruments). Crystals grew over 3 weeks in condition A11 (20% w/v PEG8000, 0.2 M Ammonium Sulphate, 0.1 M Sodium Cacodylate, pH 6.0) and were harvested in a cryo-protectant (crystallisation buffer containing 20% glycerol), flash frozen and stored under liquid nitrogen.

Diffraction experiments were carried out at beamline ID23-1 (ESRF, France) at a wavelength of 0.9763 (12.7KeV); images were collected using a Pilatus 6M detector. The final dataset in space group $P3_121$ was processed using XDS to a resolution of 3Å (Kabsch, 2010)

All data manipulation was carried out using the CCP4 suite (Winn et al., 2011). Data reduction and scaling was performed using AIMLESS (Evans and Murshudov, 2013). Molecular replacement was carried out with PHASER using pdb models 1U6A for the Fab' and 3QD6 for CD40 (McCoy et al., 2007). Iterative model building and reciprocal space refinement were carried out using COOT (Emsley et al., 2010) and REFMAC5 (Murshudov

et al., 1997). Refinement statistics are given in Table S1. The final model and structure factors have been deposited in the PDB.

NF-κB assay

DNA encoding wild-type human CD40 in the pCIpuro vector was transfected into NF-κB/Jurkat/GFP reporter cells (System Biosciences) with Lipofectamine2000 (Thermofisher). Stable transfectants were selected in 10% RPMI medium containing 1 μg/ml puromycin and single-cell cloned to establish a stable cell-line for use. To assess NF-κB activity, cells were stimulated with of anti-hCD40 mAb for 8 hours at 37 ºC and activity was measured by the production of GFP by flow cytometry.

Surface Plasmon Resonance.

A Biacore T100 was used to determine competition between pairs of anti-hCD40 mAb for binding to human CD40. hCD40-Fc (R&D Systems) was immobilised onto a CM5 chip at 1000 RU at pH5. mAb binding was analysed at 500 nM at 25ºC with a flow rate of 10 μl/min in HBS-EP+ running buffer (GE Healthcare). The first mAb was injected for 600 seconds followed by the second for 180 seconds. The chip was regenerated with 10 mM glycine pH1.5 for 30 sec at 30 μl/min. The blank control curve was automatically subtracted. Results were analysed using Biacore T100 Evaluation software and GraphPad Prism. mAb used were ChiLob 7/4 h1, SGN40 h1, CP870,893 h1, Lob 7/6 h2.

Phagocytosis assay

Bone marrow from the femurs and tibia of WT, FcγRIIB KO or γ chain KO C57BL/6 mice was resuspended at $1x10^6$ cells/ml in complete RPMI containing 20% L929 cell supernatant

and 50μM β-mercaptoethanol, and incubated for 6-8 days at 37^0C/5% CO_2. Adherent macrophages were harvested using trypsin/EDTA (Invitrogen), resuspended in complete RPMI, plated into a 96-well tissue culture plate (5×10^4/well), and incubated for 2 to 4 hours at 37^oC/5% CO_2. hCD40Tg B cells were purified as above and labelled with 5 μM CFSE before opsonising with 10 μg/ml of the indicated mAb. Opsonised B cells were then co-cultured with macrophages at a ratio of 5:1 for 30 minutes at 37°C, stained with anti-F4/80-APC and analysed by flow cytometry.

QUANTIFICATION AND STATISTICAL ANALYSIS

Students T-tests (unpaired, two-tailed) or one way ANOVA followed by Tukey's multiple comparisons test were performed using GraphPad Prism software (GraphPad Software, inc., La Jolla, California) as indicated for individual experiments. In some cases data from multiple experiments were combined.

DATA AND SOFTWARE AVAILABILITY

The CD40 ECD/ChiLob 7/4 Fab' crystal structure has been deposited in the PDB database, dataset ID: D_1200001230; PDB ID 6FAX

KEY RESOURCES TABLE

REAGENT or RESOURCE	SOURCE	IDENTIFIER
Antibodies		
Mouse IgG HRP	Dako	Cat. # PO447
Mouse CD23 PE (B3B4)	BD	Cat.# 553139; RRID:AB_394654
Mouse MHCII FITC (M5/114)	In-house	N/A
Mouse CD86 FITC (GL1)	In-house	N/A
Mouse CD8α APC (53-6.7)	BD	Cat. # 561093; RRID: AB_398527
Mouse IgG (FITC)	Abcam	Cat. # ab97264; RRID: AB_ 10688260
Penta.His	Qiagen	Cat. # 34660; RRID: AB_2619735
Human Fc HRP	Jackson ImmunoResearch	Cat. # 109-035-098; RRID: AB_2337586
Human CD23 FITC (MHM6)	In-house	N/A
Human CD40 (Lob 7/4; various isotypes; FITC)	In-house (Johnson et al, 2015)	N/A
Human CD40 (Lob 7/2; various isotypes)	In-house	N/A
Human CD40 (Lob 7/6; various isotypes; FITC)	In-house	N/A
Human CD40 (Lob 7/7; various isotypes; FITC)	In-house	N/A
Human CD40 (Lob 7/8; various isotypes; FITC)	In-house	N/A
Human CD40 (Lob 8/2; various isotypes)	In-house	N/A
Human CD40 (24.2.1; various isotypes)	In-house	N/A
Human CD40 (CP870,893; various isotypes)	In-house (Vonderheide et al, 2007)	N/A
Human CD40 (SGN40; various isotypes)	In-house (Hussein et al, 2010)	N/A
Bacterial and Virus Strains		
Biological Samples		
Chemicals, Peptides, and Recombinant Proteins		
Chicken Ovalbumin	Sigma-Aldrich	Cat. # A2512
SIINFEKL tetramer PE	In-house (White et al, 2011)	N/A
Lymphoprep	Axis-Shield	Cat. # 07861

SuperSignal West Pico Chemiluminescent Substrate	Thermo Fisher	Cat. # 34080
GenePORTER	Genlantis	T201075
Critical Commercial Assays		
EasySep™ mouse B cell isolation kit	StemCell Technologies	Cat. # 19854
EasySep™ human B cell isolation kit	StemCell Technologies	Cat. # 17954
Deposited Data		
CD40 ECD/ChiLob 7/4 Fab' crystal structure	Protein Data Bank	6FAX
Experimental Models: Cell Lines		
Freestyle™ 293-F cells	Thermo Fisher Scientific	Cat. # R79007
CHO-K1 cells	Sigma-Aldrich	Cat. # 85051005
NF-κB/Jurkat/GFP reporter cell line	System Biosciences	Cat. # TR850A-1
Experimental Models: Organisms/Strains		
Mouse: C57BL/6	Charles River Laboratories	Strain: 027
Mouse: hCD40Tg: C57BL/6-Tg(hCD40)	Gift from R Noelle (Ahonen et al, 2002)	N/A
Mouse: FcγRII$^{-/-}$: C57BL/6-*Fcgr2*$^{-/-}$	Gift from Dr Verbeek, Leiden University Medical Centre	N/A
Mouse: FcRγ chain $^{-/-}$: C57BL/6-*Fcer1g*$^{-/-}$	Gift from Dr Verbeek, Leiden University Medical Centre	N/A
Oligonucleotides		
HuCD40F: AAGCTTGGTCTCACCTCGCCATGGTTCGT		
HuCD40Ec-6HisR: CTCGAGCTAATGATGATGATGATGTCTCAGCCG ATGGTG		
Recombinant DNA		
pCIpuro	Modified in-house from PCIneo (Promega Cat. # E1841)	N/A
pEE6.4	Licensed from Lonza	N/A

pEE12.4	Licensed from Lonza	N/A
Software and Algorithms		
Prism	Graphpad	N/A
FCS Express V3	De Novo	N/A
AIMLESS	CCP4 (Evans and Murshudov, 2013)	N/A
PHASER	CCP4 (McCoy et al, 2007)	N/A
COOT	CPP4 (Emsley et al, 2010)	N/A
REFMAC5	CCP4 (Murshudov, 1997)	N/A
Other		

Figure 1

Click here to download Figure Figure 1.tif

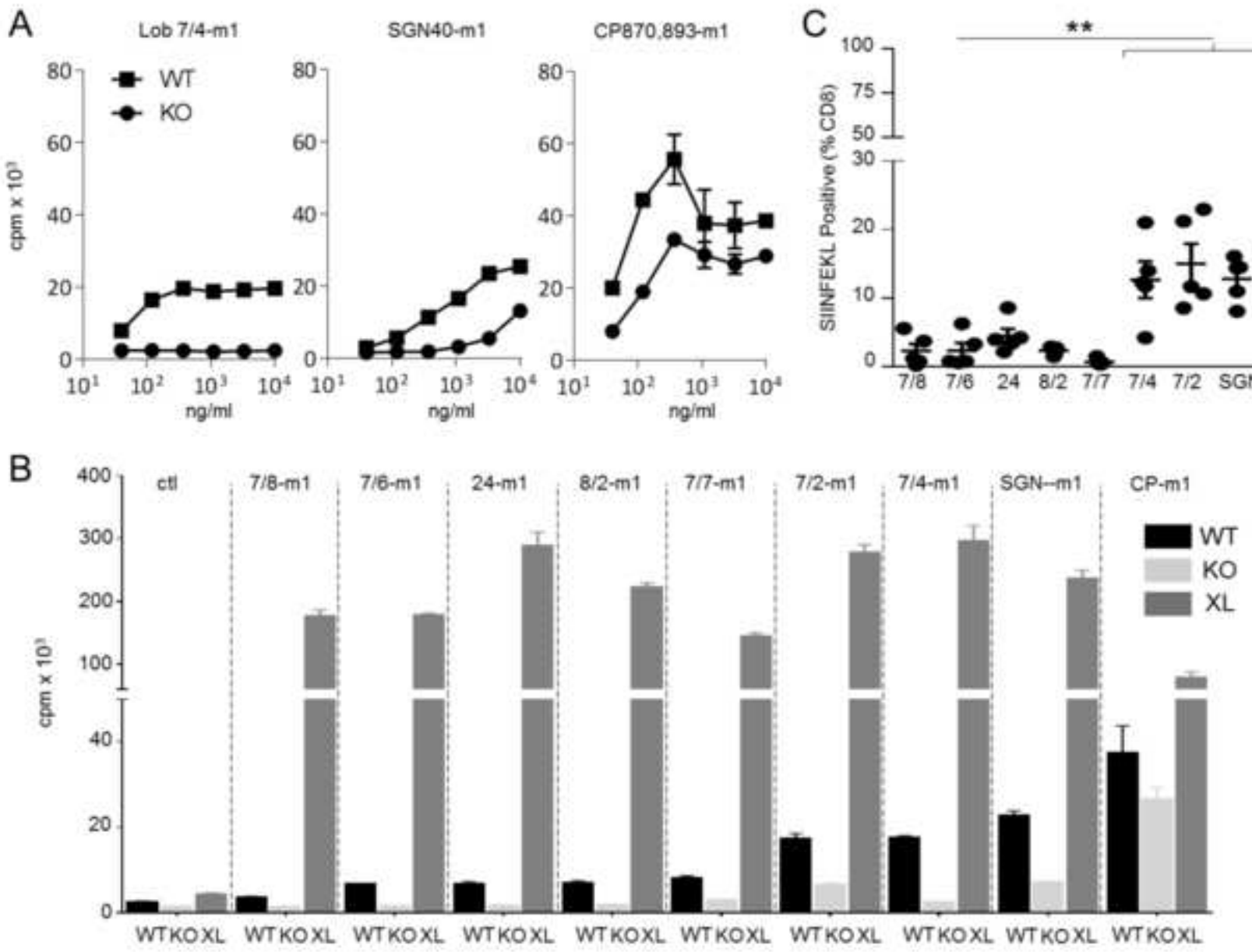

Figure 2

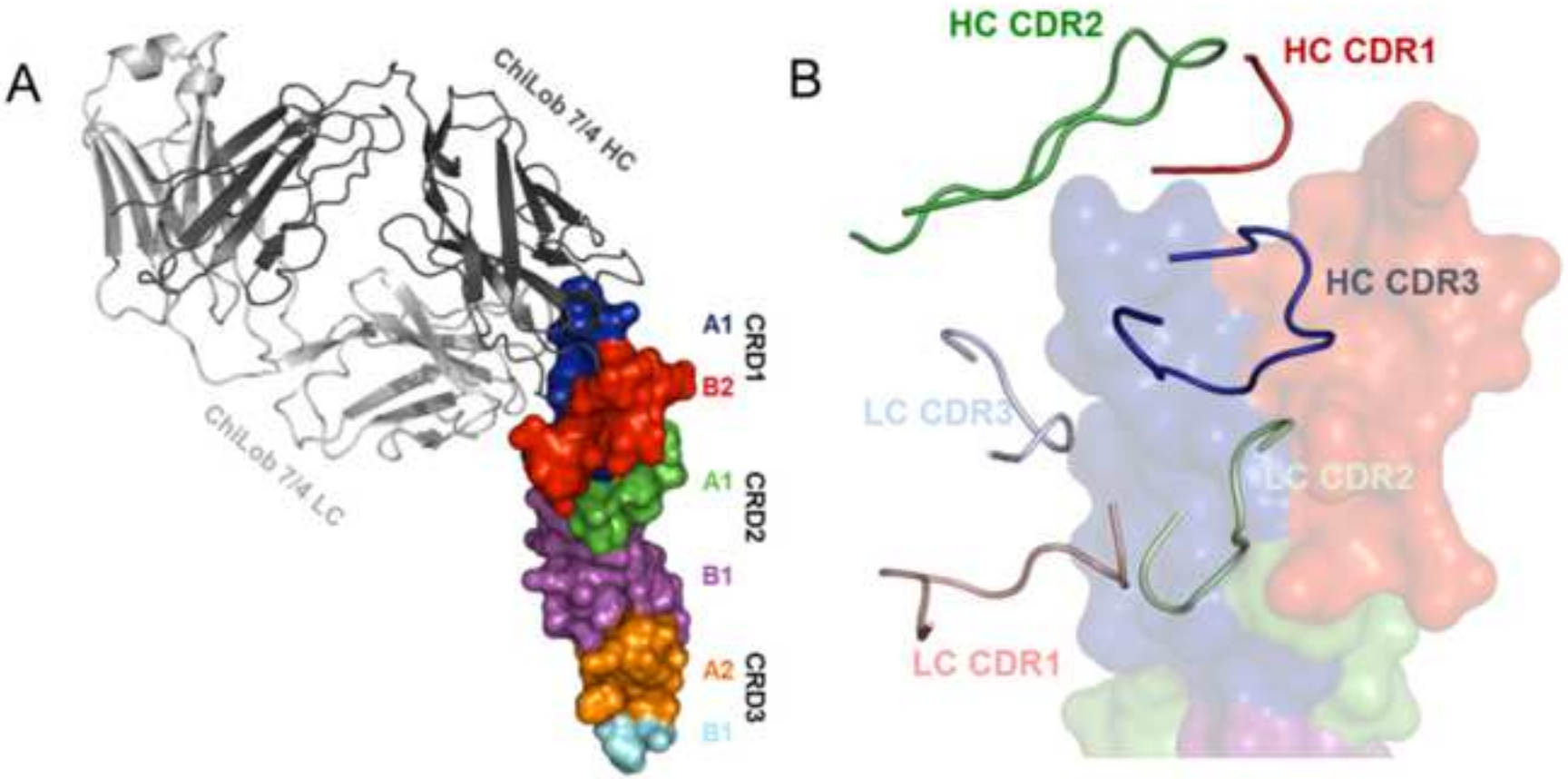

Figure 3

Click here to download Figure Figure 3.tif

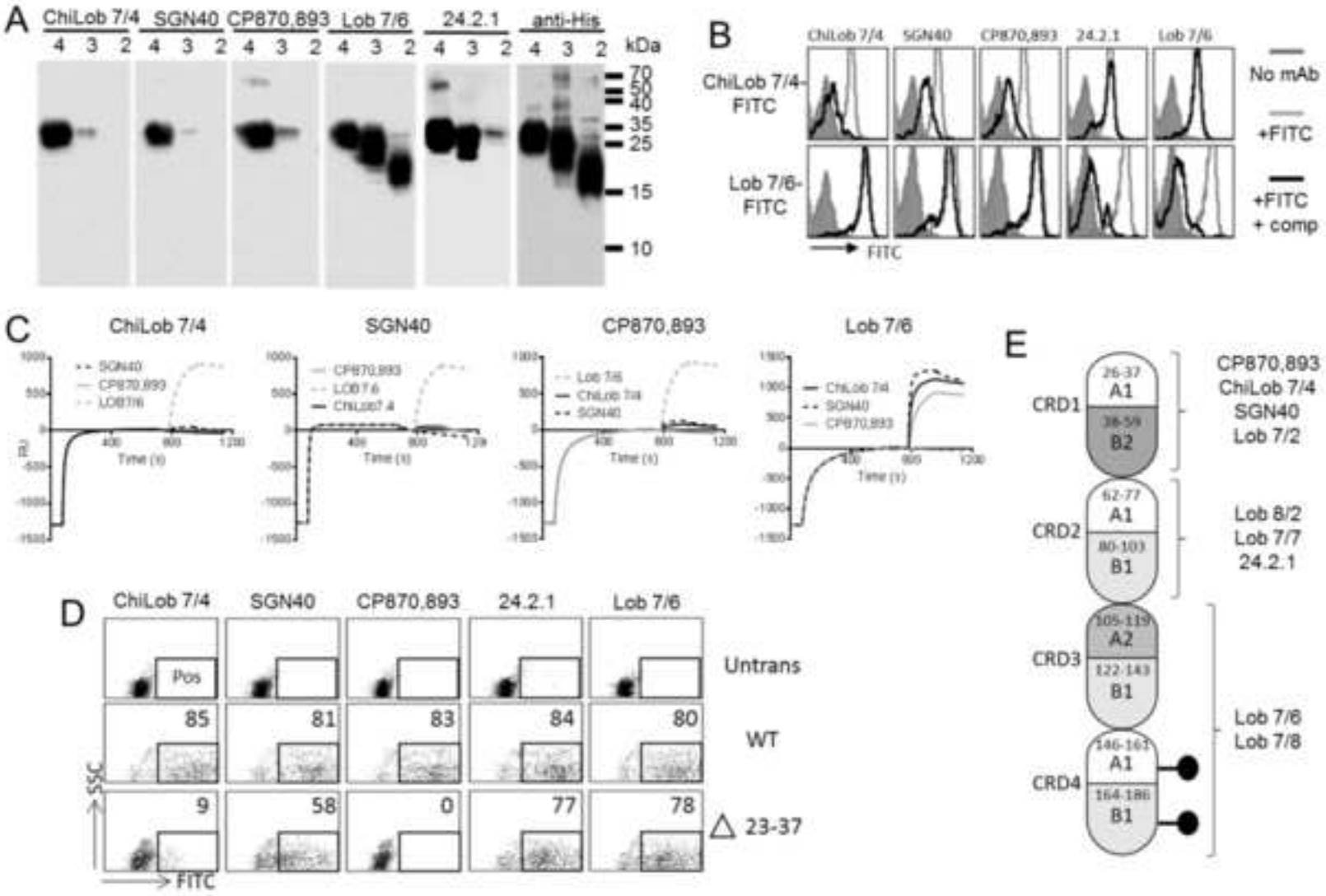

Figure 4

A

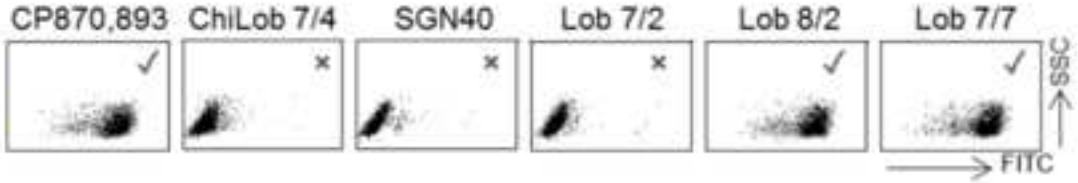

B

	CP870,893	ChiLob 7/4	SGN40	Lob 7/2	Lob 8/2	Lob 7/7
R27-E28	×	✓	✓	✓	✓	✓
T52-E53	✓	✓	×	×	✓	✓
F54-T55	✓	×	×	×	✓	✓
E56-T57	✓	✓	×	×	✓	✓
G63-E64	✓	✓	✓	✓	×	✓
D84-P85	✓	✓	✓	✓	✓	×
K94-G95	✓	✓	✓	✓	×	✓

C

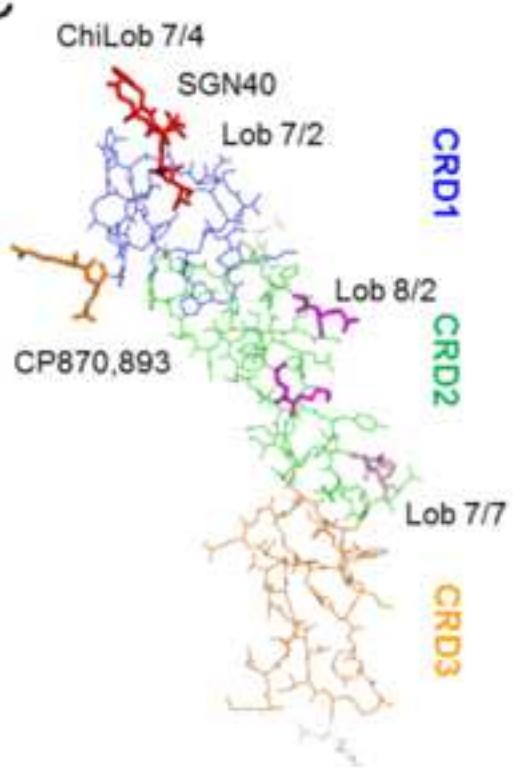

Figure 5

Click here to download Figure Figure 5.tif

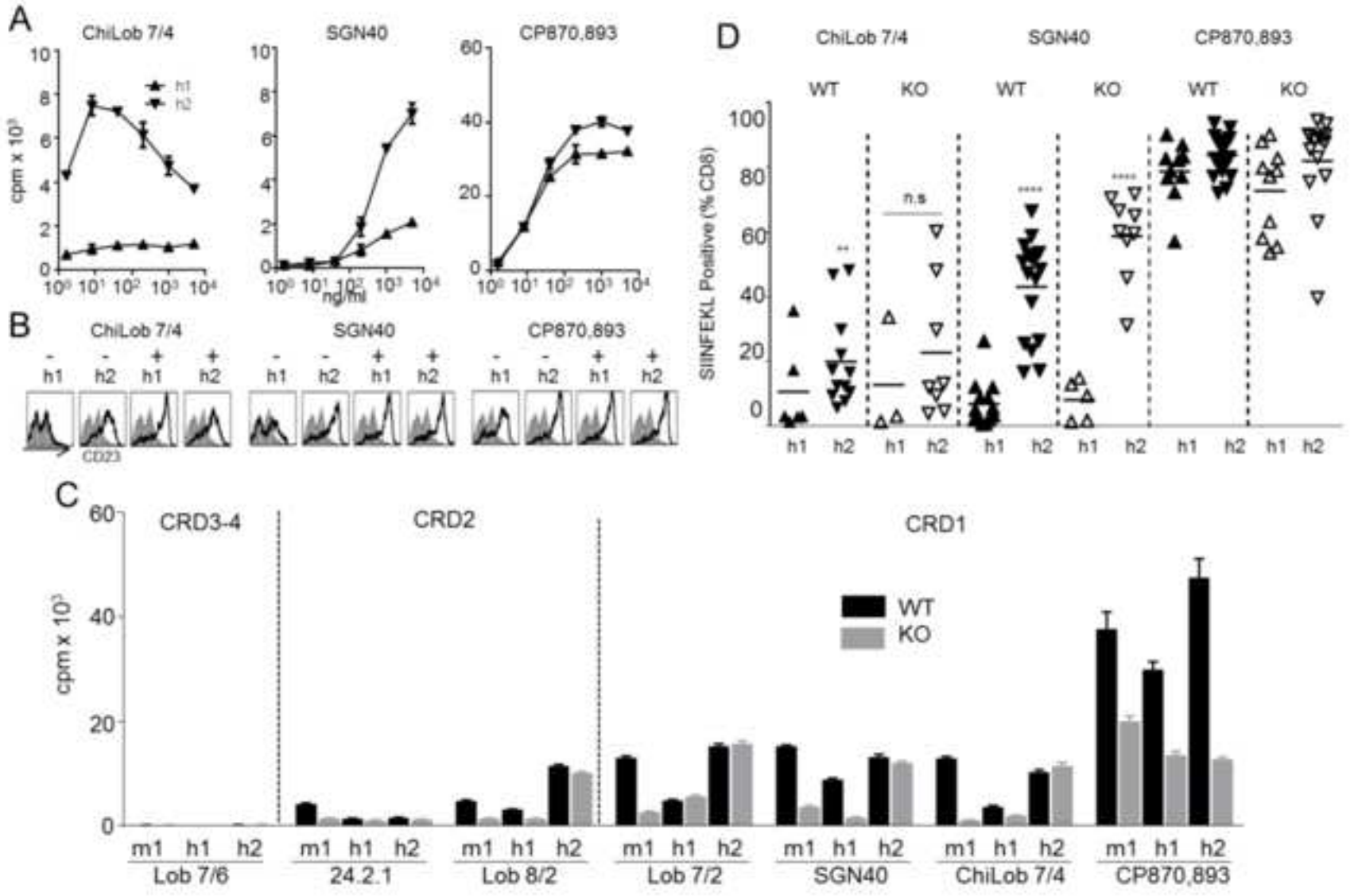

Figure 6

Click here to download Figure Figure 6.tif

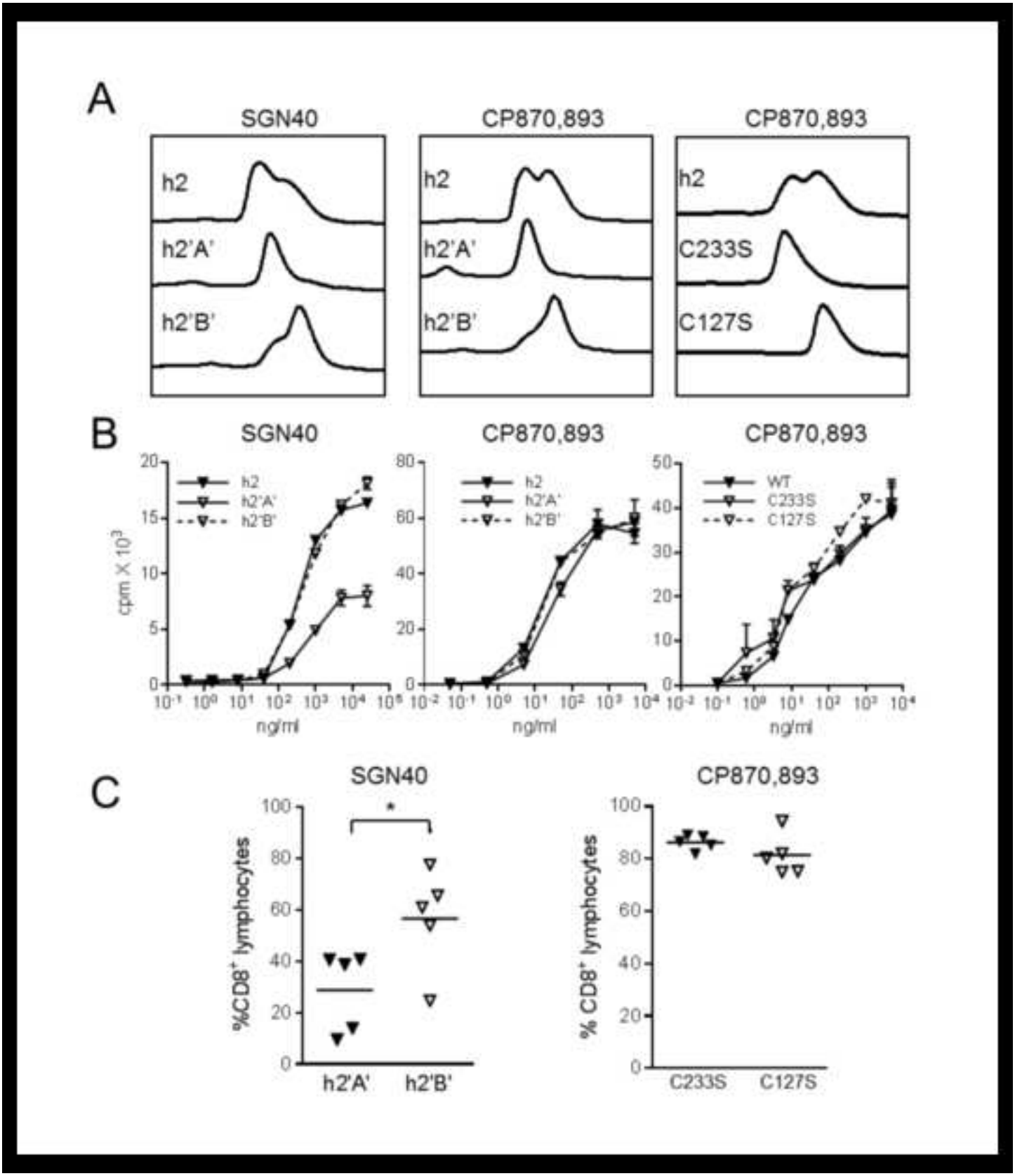

Figure 7

Click here to download Figure Figure 7.tif

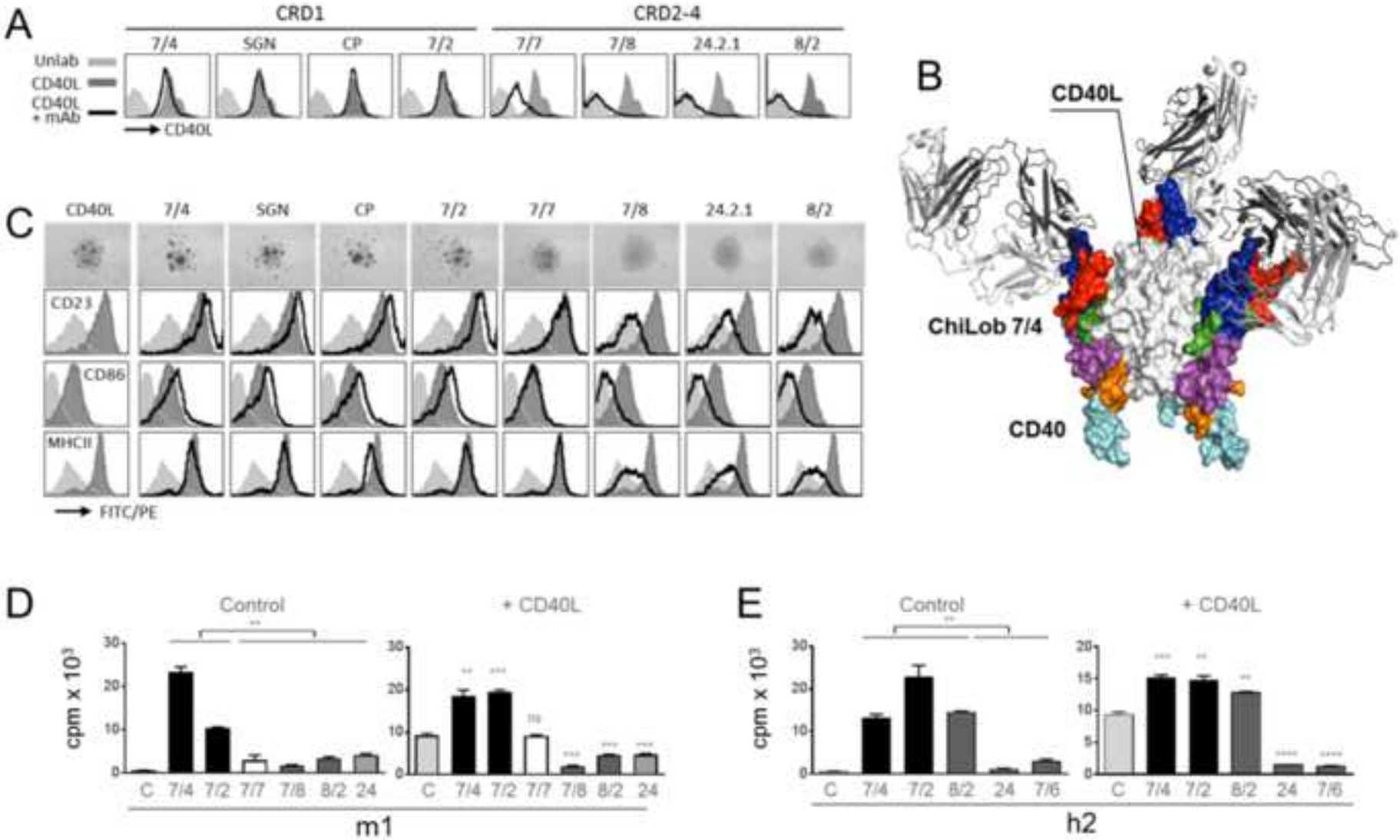

Table S1. Related to Figure 2.

	ChiLob 7/4 Fab:CD40 Complex
Data collection	
Space group	P 3_1 2 1
Cell dimensions	
a, b, c (Å)	158.75 158.75 96.62
a, b, g (°)	90 90 120
Resolution (Å)	51.96 - 3.00 (3.08-3.00)
R_{sym} or R_{merge}	0.157 (1.445)
I / sI	13.0 (32.9)
Completeness (%)	100 (98.4)
Redundancy	13.7 (11.4)
Refinement	
Resolution (Å)	3.00
No. reflections	27540
R_{work} / R_{free}	0.190 / 0.237
No. atoms	
Protein	4091
Ligand/ion	0
Water	23
B-factors	
Protein	87.03
Ligand/ion	0
Water	78.14
R.m.s. deviations	
Bond lengths (Å)	0.0169
Bond angles (°)	2.135

Data Collection and Refinement Statistics of ChiLob 7/4 Fab:CD40 Complex (PDB ID 6FAX). High resolution shell statistics shown in parenthesis. 5% of reflections were used for calculation of Rfree.

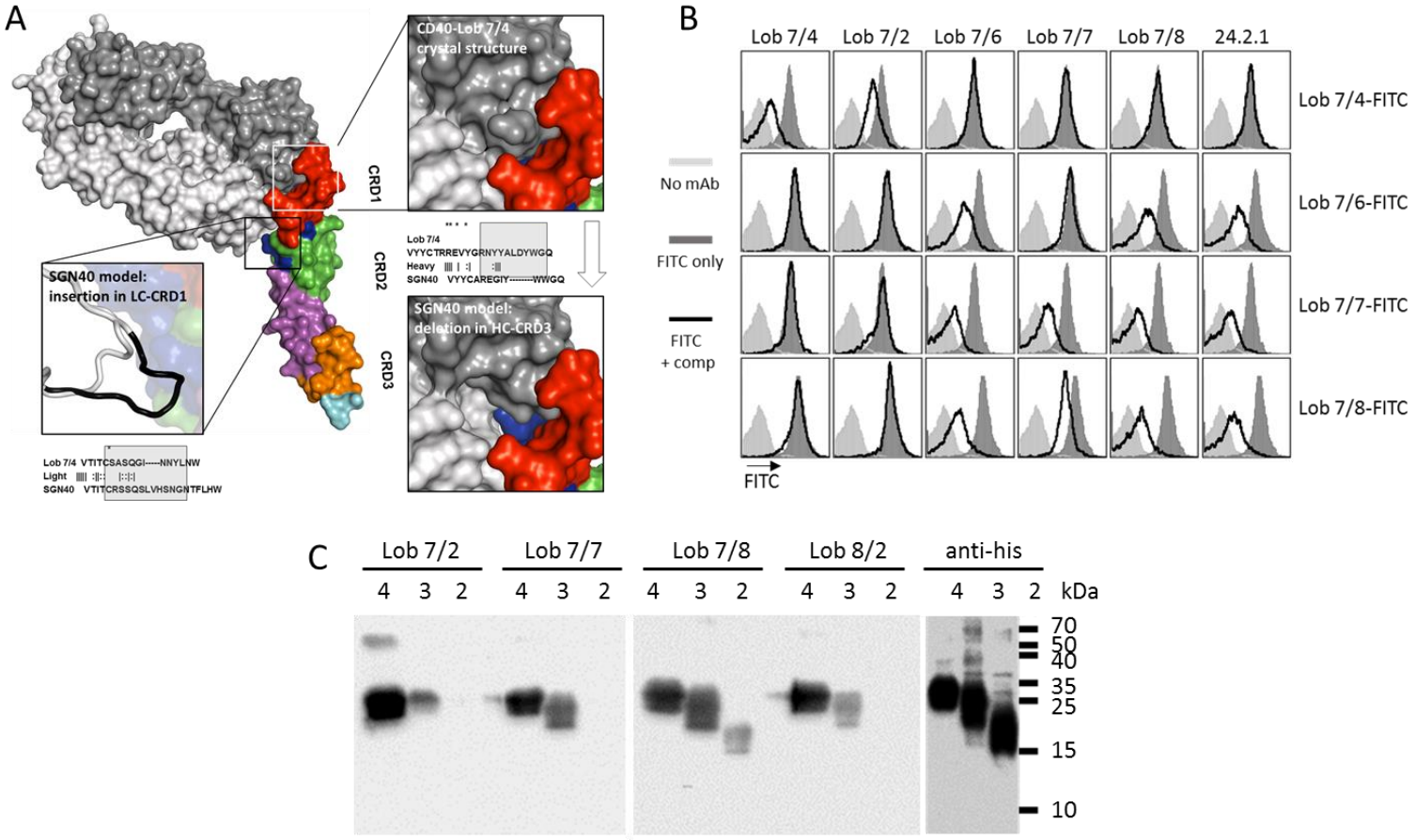

Figure S1. Epitope mapping of hCD40 mAb. Related to Figure 3. (A) Modelling of SGN40 binding onto the ChiLob 7/4:CD40 crystal structure. Surface view of the structure of the CD40:ChiLob 7/4 complex with CRD regions of CD40 coloured and mapped as in Figure 2 with various insets highlighting key parts of the interaction. Below are models produced to show the predicted structural differences apparent in the SGN40 and ChiLob 7/4 Fab based on loop length changes in the heavy chain CRD3 and the light chain CRD1. Panels: Top right panel highlights the binding of ChiLob 7/4 to CD40 in the crystal structure. Note: The LC CDR3 of ChiLob 7/4 binds into a pocket on the CRD1-B2 of CD40 and the light chain CRD1 of ChiLob 7/4 binds in a pocket of CD40 CDR1-A1. Below is shown the sequence alignment between the HC CDR3 of ChiLob 7/4 and SGN40 with the key binding residues in the structure of ChiLob 7/4 starred. Below (bottom right) shows how the 8 amino-acid deletion in the SGN40 HC would prevent it making the same interaction with the pocket of CRD1-B2 of

CD40 as ChiLob 7/4. The bottom left panel shows a modelled representation of how the 5 amino-acid insertion of the SGN40 LC CDR1 (bottom loop, black) would impair binding in this region. Below is the sequence alignment between the LC CDR1 of ChiLob 7/4 and SGN40 with the key binding residue starred. (B) hCD40Tg mouse B cells were incubated with FITC-labelled Lob 7/4, Lob 7/6, Lob 7/7 or Lob 7/8 as indicated in the absence or presence of a 10-fold excess of competitor (comp) mAb indicated above each plot. Cell labelling was assessed by flow cytometry; light grey, unlabelled cells; dark grey, FITC-labelled mAb alone; black line, FITC-labelled mAb + competitor. (C) C-terminally His-tagged CD40 proteins consisting of 4, 3, or 2 CRD domains (4 = full length; 3 = CRD1 deleted; 2 = CRD1 and 2 deleted) were analysed by Western blotting with the mAb indicated above each plot used for detection. A composite image from multiple blots is shown.

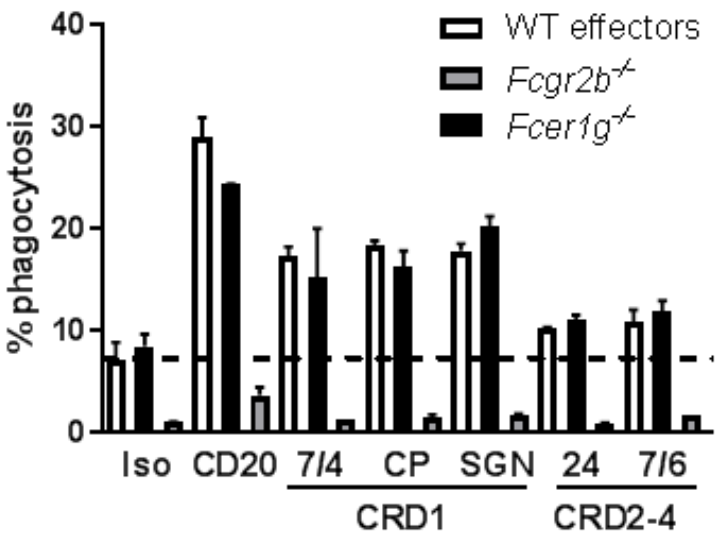

Figure S2. anti-hCD40 mAb-mediated phagocytosis. Related to Figure 4. Purified hCD40Tg mouse splenic B cells were opsonised with the indicated hCD40 mAb, mouse CD20 mAb, or isotype control, all m2a isotype, before incubation with bone marrow derived mouse macrophages from WT, *Fcgr2b*$^{-/-}$ or *Fcer1g*$^{-/-}$ mice. Phagocytosis was measured by flow cytometry as described in STAR Methods. Results (mean ± SEM) from one of 2 independent experiments are shown, * $p<0.05$ versus isotype control for WT cells.

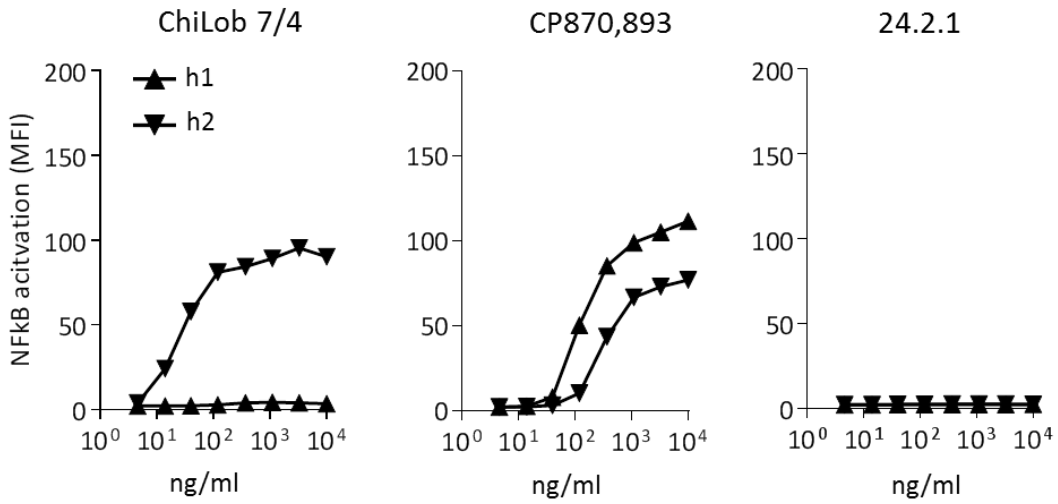

Figure S3. NF- κ B activation by anti-hCD40 mAb. Related to Figure 5. NF-κB/Jurkat/GFP reporter cells stably transfected with hCD40 were incubated with increasing concentrations of the indicated anti-hCD40 mAb of h1 or h2 isotypes for 8 hours, and then the level of NF- κ B activation was assessed by GFP quantification using flow cytometry. Mean ± SEM of triplicates, data representative of at least 2 independent experiments.

Full wwPDB X-ray Structure Validation Report (i)

Dec 18, 2017 – 11:34 AM GMT

PDB ID	:	6FAX
Title	:	Complex of Human CD40 Ectodomain with Lob 7.4 Fab
Deposited on	:	2017-12-18
Resolution	:	2.99 Å(reported)

This is a Full wwPDB X-ray Structure Validation Report.

This report is produced by the wwPDB biocuration pipeline after annotation of the structure.

We welcome your comments at *validation@mail.wwpdb.org*
A user guide is available at
http://wwpdb.org/validation/2016/XrayValidationReportHelp
with specific help available everywhere you see the (i) symbol.

The following versions of software and data (see references (1)) were used in the production of this report:

MolProbity	:	4.02b-467
Xtriage (Phenix)	:	1.9-1692
EDS	:	rb-20030345
Percentile statistics	:	20161228.v01 (using entries in the PDB archive December 28th 2016)
Refmac	:	5.8.0135
CCP4	:	6.5.0
Ideal geometry (proteins)	:	Engh & Huber (2001)
Ideal geometry (DNA, RNA)	:	Parkinson et al. (1996)
Validation Pipeline (wwPDB-VP)	:	rb-20030345

1 Overall quality at a glance (i)

The following experimental techniques were used to determine the structure:
X-RAY DIFFRACTION

The reported resolution of this entry is 2.99 Å.

Percentile scores (ranging between 0-100) for global validation metrics of the entry are shown in the following graphic. The table shows the number of entries on which the scores are based.

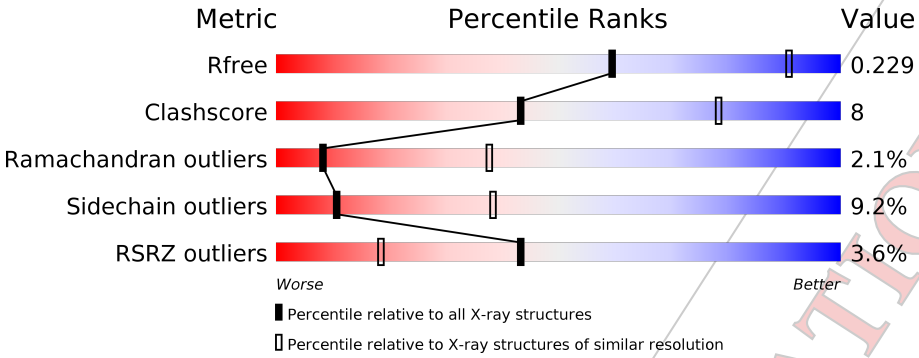

Metric	Whole archive (#Entries)	Similar resolution (#Entries, resolution range(Å))
R_{free}	100719	1692 (3.00-3.00)
Clashscore	112137	2037 (3.00-3.00)
Ramachandran outliers	110173	1973 (3.00-3.00)
Sidechain outliers	110143	1976 (3.00-3.00)
RSRZ outliers	101464	1716 (3.00-3.00)

The table below summarises the geometric issues observed across the polymeric chains and their fit to the electron density. The red, orange, yellow and green segments on the lower bar indicate the fraction of residues that contain outliers for >=3, 2, 1 and 0 types of geometric quality criteria. A grey segment represents the fraction of residues that are not modelled. The numeric value for each fraction is indicated below the corresponding segment, with a dot representing fractions <=5% The upper red bar (where present) indicates the fraction of residues that have poor fit to the electron density. The numeric value is given above the bar.

Mol	Chain	Length	Quality of chain
1	L	214	76% 21% ••
2	H	240	70% 19% 10%
3	R	173	11% 39% 14% 5% 42%

2 Entry composition

There are 4 unique types of molecules in this entry. The entry contains 4084 atoms, of which 0 are hydrogens and 0 are deuteriums.

In the tables below, the ZeroOcc column contains the number of atoms modelled with zero occupancy, the AltConf column contains the number of residues with at least one atom in alternate conformation and the Trace column contains the number of residues modelled with at most 2 atoms.

- Molecule 1 is a protein called Lob 7.4 light chain.

Mol	Chain	Residues	Atoms					ZeroOcc	AltConf	Trace
			Total	C	N	O	S			
1	L	211	1629	1018	269	337	5	0	0	0

- Molecule 2 is a protein called Lob 7.4 heavy chain.

Mol	Chain	Residues	Atoms					ZeroOcc	AltConf	Trace
			Total	C	N	O	S			
2	H	216	1648	1044	272	325	7	0	0	0

- Molecule 3 is a protein called Tumor necrosis factor receptor superfamily member 5.

Mol	Chain	Residues	Atoms					ZeroOcc	AltConf	Trace
			Total	C	N	O	S			
3	R	100	786	472	134	165	15	0	1	0

- Molecule 4 is water.

Mol	Chain	Residues	Atoms		ZeroOcc	AltConf
			Total	O		
4	L	10	10	10	0	0
4	H	8	Total	O	0	0
			8	8		
4	R	3	Total	O	0	0
			3	3		

3 Residue-property plots (i)

These plots are drawn for all protein, RNA and DNA chains in the entry. The first graphic for a chain summarises the proportions of the various outlier classes displayed in the second graphic. The second graphic shows the sequence view annotated by issues in geometry and electron density. Residues are color-coded according to the number of geometric quality criteria for which they contain at least one outlier: green = 0, yellow = 1, orange = 2 and red = 3 or more. A red dot above a residue indicates a poor fit to the electron density (RSRZ > 2). Stretches of 2 or more consecutive residues without any outlier are shown as a green connector. Residues present in the sample, but not in the model, are shown in grey.

- Molecule 1: Lob 7.4 light chain

Chain L:

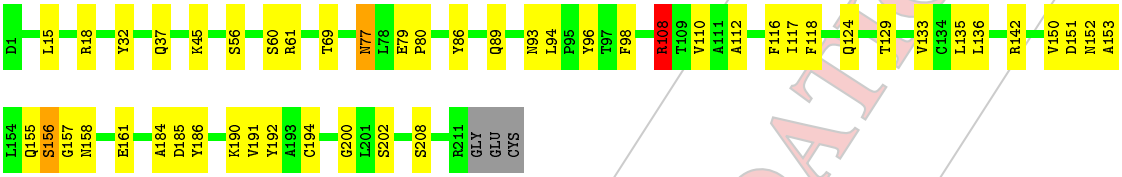

- Molecule 2: Lob 7.4 heavy chain

Chain H:

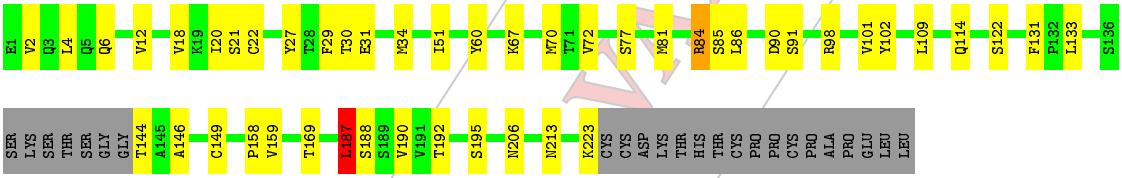

- Molecule 3: Tumor necrosis factor receptor superfamily member 5

Chain R:

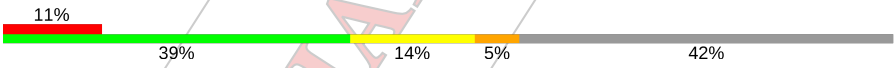

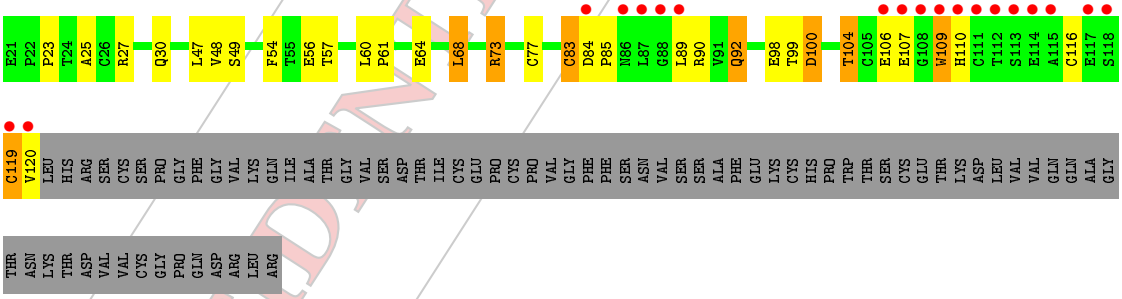

4 Data and refinement statistics (i)

Property	Value	Source
Space group	P 31 2 1	Depositor
Cell constants a, b, c, α, β, γ	158.75Å 158.75Å 93.62Å 90.00° 90.00° 120.00°	Depositor
Resolution (Å)	137.48 – 2.99 51.96 – 2.99	Depositor EDS
% Data completeness (in resolution range)	99.7 (137.48-2.99) 99.7 (51.96-2.99)	Depositor EDS
R_{merge}	0.16	Depositor
R_{sym}	(Not available)	Depositor
$< I/\sigma(I) >$ [1]	2.12 (at 3.01Å)	Xtriage
Refinement program	REFMAC 5.8.0158	Depositor
R, R_{free}	0.185 , 0.231 0.190 , 0.229	Depositor DCC
R_{free} test set	1319 reflections (5.00%)	DCC
Wilson B-factor (Å^2)	86.7	Xtriage
Anisotropy	0.040	Xtriage
Bulk solvent k_{sol}(e/Å^3), B_{sol}(Å^2)	0.32 , 52.1	EDS
L-test for twinning[2]	$< \|L\| > = 0.51$, $< L^2 > = 0.34$	Xtriage
Estimated twinning fraction	0.014 for -h,-k,l	Xtriage
F_o,F_c correlation	0.95	EDS
Total number of atoms	4084	wwPDB-VP
Average B, all atoms (Å^2)	87.0	wwPDB-VP

Xtriage's analysis on translational NCS is as follows: *The largest off-origin peak in the Patterson function is 3.64% of the height of the origin peak. No significant pseudotranslation is detected.*

[1] Intensities estimated from amplitudes.

[2] Theoretical values of $< |L| >$, $< L^2 >$ for acentric reflections are 0.5, 0.333 respectively for untwinned datasets, and 0.375, 0.2 for perfectly twinned datasets.

5 Model quality

5.1 Standard geometry

The Z score for a bond length (or angle) is the number of standard deviations the observed value is removed from the expected value. A bond length (or angle) with $|Z| > 5$ is considered an outlier worth inspection. RMSZ is the root-mean-square of all Z scores of the bond lengths (or angles).

Mol	Chain	Bond lengths		Bond angles	
		RMSZ	#$\|Z\|>5$	RMSZ	#$\|Z\|>5$
1	L	0.84	0/1663	1.03	3/2261 (0.1%)
2	H	0.86	0/1688	0.99	2/2296 (0.1%)
3	R	1.03	0/802	1.18	3/1088 (0.3%)
All	All	0.89	0/4153	1.04	8/5645 (0.1%)

Chiral center outliers are detected by calculating the chiral volume of a chiral center and verifying if the center is modelled as a planar moiety or with the opposite hand.A planarity outlier is detected by checking planarity of atoms in a peptide group, atoms in a mainchain group or atoms of a sidechain that are expected to be planar.

Mol	Chain	#Chirality outliers	#Planarity outliers
3	R	0	2

There are no bond length outliers.

All (8) bond angle outliers are listed below:

Mol	Chain	Res	Type	Atoms	Z	Observed(^{o})	Ideal(^{o})
3	R	109	TRP	CA-CB-CG	7.04	127.07	113.70
2	H	187	LEU	CA-CB-CG	6.60	130.49	115.30
1	L	110	VAL	CB-CA-C	-6.51	99.04	111.40
3	R	119	CYS	CA-CB-SG	6.20	125.15	114.00
2	H	81	MET	CG-SD-CE	-6.06	90.50	100.20
1	L	108	ARG	NE-CZ-NH1	6.04	123.32	120.30
1	L	96	TYR	CB-CG-CD1	5.86	124.52	121.00
3	R	73	ARG	NE-CZ-NH1	5.45	123.03	120.30

There are no chirality outliers.

All (2) planarity outliers are listed below:

Mol	Chain	Res	Type	Group
3	R	106	GLU	Peptide
3	R	83	CYS	Peptide

5.2 Too-close contacts (i)

In the following table, the Non-H and H(model) columns list the number of non-hydrogen atoms and hydrogen atoms in the chain respectively. The H(added) column lists the number of hydrogen atoms added and optimized by MolProbity. The Clashes column lists the number of clashes within the asymmetric unit, whereas Symm-Clashes lists symmetry related clashes.

Mol	Chain	Non-H	H(model)	H(added)	Clashes	Symm-Clashes
1	L	1629	0	1573	25	0
2	H	1648	0	1620	27	0
3	R	786	0	699	16	0
4	H	8	0	0	0	0
4	L	10	0	0	1	0
4	R	3	0	0	0	0
All	All	4084	0	3892	61	0

The all-atom clashscore is defined as the number of clashes found per 1000 atoms (including hydrogen atoms). The all-atom clashscore for this structure is 8.

All (61) close contacts within the same asymmetric unit are listed below, sorted by their clash magnitude.

Atom-1	Atom-2	Interatomic distance (Å)	Clash overlap (Å)
3:R:27:ARG:HB2	3:R:30:GLN:HE21	1.63	0.63
2:H:12:VAL:HG21	2:H:86:LEU:HD13	1.84	0.59
1:L:150:VAL:HG13	1:L:192:TYR:CE1	2.38	0.59
2:H:18:VAL:HG12	2:H:86:LEU:HD11	1.85	0.57
2:H:2:VAL:HG23	2:H:27:TYR:CD2	2.39	0.57
1:L:118:PHE:CD2	2:H:133:LEU:HB3	2.40	0.56
3:R:27:ARG:CB	3:R:30:GLN:HE21	2.19	0.56
2:H:67:LYS:CE	2:H:90:ASP:OD2	2.54	0.55
1:L:61:ARG:HD2	1:L:77:ASN:O	2.07	0.55
2:H:67:LYS:HE3	2:H:90:ASP:OD2	2.08	0.53
2:H:29:PHE:HB2	2:H:77:SER:HB2	1.91	0.53
1:L:32:TYR:CE1	3:R:56:GLU:HG2	2.45	0.52
1:L:108:ARG:HH11	1:L:108:ARG:HG3	1.74	0.52
2:H:2:VAL:HG23	2:H:27:TYR:HD2	1.74	0.52
1:L:136:LEU:N	1:L:136:LEU:HD12	2.24	0.52
1:L:156:SER:O	1:L:158:ASN:N	2.42	0.52
1:L:186:TYR:HA	1:L:192:TYR:OH	2.10	0.51
3:R:27:ARG:HB3	3:R:30:GLN:CG	2.41	0.51
1:L:37:GLN:HG3	1:L:86:TYR:CE1	2.45	0.51
1:L:112:ALA:HB2	1:L:200:GLY:O	2.10	0.51
1:L:124:GLN:HG3	2:H:131:PHE:CE2	2.47	0.50

Continued on next page...

Continued from previous page...

Atom-1	Atom-2	Interatomic distance (Å)	Clash overlap (Å)
1:L:186:TYR:CD1	1:L:192:TYR:CE2	3.00	0.50
1:L:155:GLN:N	1:L:155:GLN:HE21	2.10	0.50
3:R:47:LEU:HD12	3:R:48:VAL:N	2.27	0.50
2:H:29:PHE:HE2	2:H:72:VAL:CG1	2.25	0.49
2:H:6:GLN:H	2:H:114:GLN:HE22	1.58	0.49
1:L:108:ARG:HG3	1:L:108:ARG:NH1	2.27	0.49
1:L:202:SER:N	4:L:301:HOH:O	2.46	0.49
3:R:92:GLN:HE21	3:R:92:GLN:C	2.16	0.49
3:R:104:THR:HA	3:R:116:CYS:SG	2.53	0.49
3:R:68:LEU:HD22	3:R:77:CYS:HA	1.96	0.48
2:H:51:ILE:HD13	2:H:72:VAL:HG23	1.95	0.47
2:H:67:LYS:HE2	2:H:90:ASP:OD2	2.15	0.47
1:L:153:ALA:O	1:L:155:GLN:NE2	2.48	0.47
3:R:60:LEU:HG	3:R:61:PRO:HD2	1.97	0.46
1:L:117:ILE:HD12	1:L:194:CYS:HB2	1.97	0.46
2:H:6:GLN:HA	2:H:21:SER:O	2.16	0.46
1:L:192:TYR:O	1:L:208:SER:HA	2.16	0.45
1:L:94:LEU:HD21	3:R:54:PHE:HB3	1.98	0.45
2:H:12:VAL:CG2	2:H:86:LEU:HD13	2.46	0.45
2:H:102:TYR:HB3	3:R:23:PRO:HD3	1.98	0.45
2:H:84:ARG:HG3	2:H:85:SER:HB2	1.99	0.45
2:H:6:GLN:N	2:H:114:GLN:HE22	2.15	0.44
3:R:109:TRP:HB3	3:R:119:CYS:HB3	1.99	0.44
2:H:29:PHE:CE2	2:H:72:VAL:CG1	3.01	0.44
2:H:187:LEU:C	2:H:187:LEU:HD23	2.38	0.43
1:L:108:ARG:HH11	1:L:108:ARG:CG	2.32	0.43
2:H:4:LEU:N	2:H:4:LEU:HD12	2.32	0.43
2:H:31:GLU:O	2:H:101:VAL:HG12	2.17	0.43
2:H:60:TYR:CE1	2:H:70:MET:CE	3.02	0.42
1:L:135:LEU:HD22	2:H:190:VAL:HG11	2.00	0.42
1:L:89:GLN:HB2	1:L:98:PHE:CD2	2.55	0.42
2:H:98:ARG:O	2:H:109:LEU:HA	2.19	0.41
2:H:4:LEU:HB3	2:H:22:CYS:SG	2.60	0.41
1:L:116:PHE:CD2	2:H:146:ALA:HB3	2.55	0.41
3:R:99:THR:O	3:R:100:ASP:CB	2.68	0.41
3:R:56:GLU:HG3	3:R:57:THR:N	2.36	0.41
3:R:27:ARG:HB3	3:R:30:GLN:HG3	2.03	0.40
1:L:155:GLN:HB3	1:L:158:ASN:OD1	2.21	0.40
1:L:79:GLU:HB3	1:L:80:PRO:HD2	2.03	0.40
3:R:84:ASP:O	3:R:85:PRO:C	2.60	0.40

There are no symmetry-related clashes.

5.3 Torsion angles

5.3.1 Protein backbone

In the following table, the Percentiles column shows the percent Ramachandran outliers of the chain as a percentile score with respect to all X-ray entries followed by that with respect to entries of similar resolution.

The Analysed column shows the number of residues for which the backbone conformation was analysed, and the total number of residues.

Mol	Chain	Analysed	Favoured	Allowed	Outliers	Percentiles
1	L	209/214 (98%)	192 (92%)	12 (6%)	5 (2%)	7 34
2	H	212/240 (88%)	197 (93%)	13 (6%)	2 (1%)	20 62
3	R	99/173 (57%)	81 (82%)	14 (14%)	4 (4%)	3 20
All	All	520/627 (83%)	470 (90%)	39 (8%)	11 (2%)	8 38

All (11) Ramachandran outliers are listed below:

Mol	Chain	Res	Type
1	L	56	SER
1	L	157	GLY
2	H	158	PRO
3	R	64	GLU
3	R	107	GLU
1	L	184	ALA
2	H	213	ASN
1	L	151	ASP
3	R	100	ASP
3	R	25	ALA
1	L	77	ASN

5.3.2 Protein sidechains

In the following table, the Percentiles column shows the percent sidechain outliers of the chain as a percentile score with respect to all X-ray entries followed by that with respect to entries of similar resolution.

The Analysed column shows the number of residues for which the sidechain conformation was analysed, and the total number of residues.

Mol	Chain	Analysed	Rotameric	Outliers	Percentiles
1	L	188/190 (99%)	172 (92%)	16 (8%)	12 43

Continued on next page...

Continued from previous page...

Mol	Chain	Analysed	Rotameric	Outliers	Percentiles
2	H	188/209 (90%)	172 (92%)	16 (8%)	12 43
3	R	94/157 (60%)	83 (88%)	11 (12%)	6 25
All	All	470/556 (84%)	427 (91%)	43 (9%)	11 39

All (43) residues with a non-rotameric sidechain are listed below:

Mol	Chain	Res	Type
1	L	15	LEU
1	L	18	ARG
1	L	45	LYS
1	L	60	SER
1	L	69	THR
1	L	93	ASN
1	L	108	ARG
1	L	129	THR
1	L	133	VAL
1	L	142	ARG
1	L	152	ASN
1	L	156	SER
1	L	161	GLU
1	L	185	ASP
1	L	190	LYS
1	L	191	VAL
2	H	20	ILE
2	H	30	THR
2	H	34	MET
2	H	84	ARG
2	H	91	SER
2	H	122	SER
2	H	144	THR
2	H	149	CYS
2	H	159	VAL
2	H	169	THR
2	H	187	LEU
2	H	188	SER
2	H	192	THR
2	H	195	SER
2	H	206	ASN
2	H	223	LYS
3	R	49	SER
3	R	68	LEU

Continued on next page...

Continued from previous page...

Mol	Chain	Res	Type
3	R	73	ARG
3	R	83	CYS
3	R	89	LEU
3	R	90	ARG
3	R	92	GLN
3	R	98	GLU
3	R	104	THR
3	R	110	HIS
3	R	120	VAL

Some sidechains can be flipped to improve hydrogen bonding and reduce clashes. All (8) such sidechains are listed below:

Mol	Chain	Res	Type
1	L	31	ASN
1	L	93	ASN
1	L	155	GLN
1	L	198	HIS
2	H	54	ASN
2	H	114	GLN
3	R	30	GLN
3	R	92	GLN

5.3.3 RNA (i)

There are no RNA molecules in this entry.

5.4 Non-standard residues in protein, DNA, RNA chains (i)

There are no non-standard protein/DNA/RNA residues in this entry.

5.5 Carbohydrates (i)

There are no carbohydrates in this entry.

5.6 Ligand geometry (i)

There are no ligands in this entry.

5.7 Other polymers (i)

There are no such residues in this entry.

5.8 Polymer linkage issues (i)

There are no chain breaks in this entry.

6 Fit of model and data

6.1 Protein, DNA and RNA chains

In the following table, the column labelled '#RSRZ> 2' contains the number (and percentage) of RSRZ outliers, followed by percent RSRZ outliers for the chain as percentile scores relative to all X-ray entries and entries of similar resolution. The OWAB column contains the minimum, median, 95^{th} percentile and maximum values of the occupancy-weighted average B-factor per residue. The column labelled 'Q< 0.9' lists the number of (and percentage) of residues with an average occupancy less than 0.9.

Mol	Chain	Analysed	<RSRZ>	#RSRZ>2	OWAB(Å^2)	Q<0.9
1	L	211/214 (98%)	-0.16	0 100 100	56, 78, 108, 130	0
2	H	216/240 (90%)	-0.09	0 100 100	55, 82, 114, 148	0
3	R	100/173 (57%)	0.54	19 (19%) 1 1	62, 97, 166, 192	0
All	All	527/627 (84%)	0.00	19 (3%) 43 18	55, 82, 131, 192	0

All (19) RSRZ outliers are listed below:

Mol	Chain	Res	Type	RSRZ
3	R	114	GLU	3.7
3	R	109	TRP	3.6
3	R	88	GLY	3.5
3	R	84	ASP	3.5
3	R	108	GLY	3.3
3	R	110	HIS	3.1
3	R	119	CYS	3.1
3	R	112	THR	3.0
3	R	120	VAL	2.7
3	R	118	SER	2.7
3	R	86	ASN	2.5
3	R	89	LEU	2.5
3	R	106	GLU	2.5
3	R	107	GLU	2.4
3	R	117	GLU	2.4
3	R	111	CYS	2.3
3	R	87	LEU	2.3
3	R	115	ALA	2.1
3	R	113	SER	2.0

6.2 Non-standard residues in protein, DNA, RNA chains (i)

There are no non-standard protein/DNA/RNA residues in this entry.

6.3 Carbohydrates (i)

There are no carbohydrates in this entry.

6.4 Ligands (i)

There are no ligands in this entry.

6.5 Other polymers (i)

There are no such residues in this entry.